Theoretical and numerical assessments of spin-flip time-dependent density functional theory

Zhendong Li and Wenjian Liu

Citation: The Journal of Chemical Physics **136**, 024107 (2012); doi: 10.1063/1.3676736
View online: http://dx.doi.org/10.1063/1.3676736
View Table of Contents: http://aip.scitation.org/toc/jcp/136/2
Published by the American Institute of Physics

Theoretical and numerical assessments of spin-flip time-dependent density functional theory

Zhendong Li and Wenjian Liu[a)]
Beijing National Laboratory for Molecular Sciences, Institute of Theoretical and Computational Chemistry, State Key Laboratory of Rare Earth Materials Chemistry and Applications, College of Chemistry and Molecular Engineering, and Center for Computational Science and Engineering, Peking University, Beijing 100871, People's Republic of China

(Received 18 November 2011; accepted 23 December 2011; published online 12 January 2012)

Spin-flip time-dependent density functional theory (SF-TD-DFT) with the full noncollinear hybrid exchange-correlation kernel and its approximate variants are critically assessed, both formally and numerically. As demonstrated by the ethylene torsion and the C_{2v} ring-opening of oxirane, SF-TD-DFT is very useful for describing nearly degenerate situations. However, it may occasionally yield unphysical results. This stems from the noncollinear form of the generalized gradient approximation, which becomes numerically instable in the presence of spin-flip excitations from the closed- to vacant-shell orbitals of an open-shell reference. To cure this defect, a simple modification, dubbed as ALDA0, is proposed in the spirit of adiabatic local density approximation (ALDA). It is applicable to all kinds of density functionals and yields stable results without too much loss of accuracy. In particular, the combination of ALDA0 with the Tamm-Dancoff approximation is a promising tool for studying global potential energy surfaces. In addition to the kernel problem, SF-TD-DFT is also rather sensitive to the choice of reference states, as demonstrated by the spin multiplet states of closed-shell molecules of H_2O, CH_2O, and C_2H_4. Surprisingly, SF-TD-DFT with pure density functionals may also fail for valance excitations with large orbital overlaps, at variance with the spin-conserving counterpart (SC-TD-DFT). In this case, the inclusion of a large amount of Hartree-Fock exchange is mandatory for quantitative results. Nonetheless, for spatially degenerate cases such as CF, CH, and NH^+, SF-TD-DFT is more advantageous than SC-TD-DFT, unless the latter is also space adapted. These findings are very instructive for future development and applications of TD-DFT. © *2012 American Institute of Physics*. [doi:10.1063/1.3676736]

I. INTRODUCTION

Thanks to its high performance-cost ratio, adiabatic time-dependent density functional theory (TD-DFT) has in the last two decades emerged as a powerful tool for singly excited states of molecular systems. In particular, by starting with a suitable high-spin open-shell reference, the spin-flip variant (SF-TD-DFT) can also access a class of double excitations necessary for describing spatially degenerate or nearly degenerate situations with strong nondynamical correlation, which have otherwise plagued the spin-conserving counterpart (SC-TD-DFT). The first implementation of SF-TD-DFT by Shao *et al.*[1] was based on the Tamm-Dancoff approximation (TDA) and a collinear hybrid exchange-correlation (XC) kernel and was applied to single-bond dissociations and singlet-triplet gaps of diradicals. The same idea was also adopted by Minezawa and Gordon[2] for conical intersections between the ground state and excited states that cannot be handled at all by SC-TD-DFT due to lack of interaction between the ground and the excited states.[3] However, despite of such interesting applications, the underlying collinear approximation is defective for an obvious reason: Only the Hartree-Fock (HF) exchange part of the XC kernel is responsible, whereas the pure density functional part is ineffective for the spin-flip transitions. Taking a singlet-triplet transition as an example, the collinear hybrid XC kernel for the $M_s = 0$ component of the triplet state consists of contributions from both the HF exchange and the pure density functional parts, while that for the $M_s = \pm 1$ components includes only the HF exchange portion. On one hand, this collinear approximation excludes the use of pure density functionals by which the calculated spin-flip excitation energies are simply the orbital energy differences. On the other hand, for a reasonable estimate of spin-flip excitation energies, the amount of HF exchange in the collinear kernel has to be increased to 50% or more, significantly larger than that used for ground state properties ($\sim$25%). It has been understood only recently that such empirically increased HF exchange is to mimic a fundamental symmetry, the energetic degeneracy of different components of a spin multiplet.[4,5]

A major step forward in the formulation of nonrelativistic SF-TD-DFT stems from the introduction of the so-called "noncollinear XC kernel",[6,7] a concept that was first proposed in the context of relativistic TD-DFT.[8–11] The former arises naturally from the latter upon neglecting the spin-orbit couplings. This noncollinear SF-TD-DFT in conjunction with the adiabatic local density approximation (ALDA) has successfully been applied to spin multiplet splittings[7] and geometry

a)Author to whom correspondence should be addressed. Electronic mail: liuwj@pku.edu.cn.

optimizations.[12] However, as shown by a recent study,[13] the noncollinear ALDA kernel may still fail miserably: The errors for the C_{2v} ring-opening of oxirane (H_2COCH_2) can be as large as 2 eV depending on the geometry. Full noncollinear hybrid XC kernels were implemented only rather recently by Rinkevicius *et al.*[14,15] but within TDA instead of the full SF-TD-DFT. Therefore, the full SF-TD-DFT with the full noncollinear hybrid XC kernels still remains to be implemented to reveal its full potential.

As a matter of fact, not only the implementation of SF-TD-DFT is not yet completed but also the problems inherent in the formalism itself have not been fully scrutinized. One particular issue is the spin contamination in the excited states.[4,16] If the (spatial) orbitals of a high-spin open-shell state are classified into closed-shell (C), open-shell (O), and vacant-shell (V) ones, only the CV($\beta\alpha$) (i.e., single transition from a closed-shell β orbital to a vacant-shell α orbital) type of flip-up transitions and the OO($\alpha\beta$) type of flip-down transitions can be properly described by the current implementations of SF-TD-DFT.[1–3,6,7,12–15] This is solely because such transitions are automatically spin-adapted. In contrast, the other types of flip-down single transitions, including CV($\alpha\beta$), CO($\alpha\beta$), and OV($\alpha\beta$), can lead to severely spin-contaminated states[4] (for details, see Table I of Ref. 5). Therefore, the spin-adapted variant[4] of SF-TD-DFT has to be invoked for such transitions. However, the formalism[4] is rather involved and still requires further theoretical analysis before actual applications can be made, given that it will reduce automatically to the simple spin-complete spin-flip configuration-interaction-singles approach[17] if the TDA is invoked for excitations from a HF triplet state. Another issue deserving to be mentioned here is that the results of SF-TD-DFT may be very sensitive to the choice of reference states due to lack of orbital relaxations.

Having noticed these issues, we decide to implement and analyze the full SF-TD-DFT in conjunction with the full noncollinear form of hybrid XC kernels. The numerical instabilities associated with the GGA (generalized gradient approximation) kernels are first to be addressed. The performance of SF-TD-DFT on spatially nearly degenerate situations is then examined by calculating the potential energy curves (PECs) of the ethylene torsion and the C_{2v} ring-opening of oxirane. The dependence of SF-TD-DFT on the functionals and the references is to be revealed by calculating the singlet-triplet gaps of prototypical closed-shell molecules (H_2O, CH_2O, and C_2H_4). As representatives of open-shell systems, the spin multiplet states of the CF, CH, and NH^+ molecules are finally investigated with SF-TD-DFT, SC-TD-DFT, X-TD-DFT,[18] and unrestricted-Kohn-Sham-based TD-DFT (U-TD-DFT). Note that X-TD-DFT is an extension of the spin-adapted SC-TD-DFT (Refs. 4, 5) by further incorporating the spin-degeneracy conditions and simultaneously removing the double counting of correlation for those already spin-adapted states. Similar corrections should, in principle, be applied also to SF-TD-DFT. However, since only the CV($\beta\alpha$) and OO($\alpha\beta$) types of spin-flip excitations are to be investigated here, such corrections have no discernible effects (less than 0.02 eV) and hence will not be considered.

II. THEORY

The following convention for labeling the molecular orbitals is used throughout: $\{i, j, k, l, \dots\}$ for doubly occupied, $\{a, b, c, d, \dots\}$ for unoccupied, and $\{p, q, r, s, \dots\}$ for unspecified orbitals. Greek indices are used to denote electron spin. Moreover, all the orbitals are assumed to be real-valued since spin-orbit couplings are not under concern here. Adiabatic TD-DFT then amounts to solving the following eigenvalue problem:

$$\begin{bmatrix} \mathbf{A} & \mathbf{B} \\ \mathbf{B} & \mathbf{A} \end{bmatrix} \begin{bmatrix} \mathbf{X} \\ \mathbf{Y} \end{bmatrix} = \omega \begin{bmatrix} \mathbf{I} & \mathbf{0} \\ \mathbf{0} & -\mathbf{I} \end{bmatrix} \begin{bmatrix} \mathbf{X} \\ \mathbf{Y} \end{bmatrix}, \tag{1}$$

where the orbital Hessian matrices $\mathbf{A}$ and $\mathbf{B}$ are defined as

$$[\mathbf{A}^{\sigma\tau,\sigma'\tau'}]_{pq,rs} = \delta_{\sigma\sigma'}\delta_{\tau\tau'}\left(\delta_{qs}F^{\sigma}_{pr} - \delta_{pr}F^{\tau}_{sq}\right) + [K^{\sigma\tau,\sigma'\tau'}]_{pq,rs}, \tag{2}$$

$$[\mathbf{B}^{\sigma\tau,\sigma'\tau'}]_{pq,rs} = [K^{\sigma\tau,\tau'\sigma'}]_{pq,sr}, \tag{3}$$

in terms of canonical or localized molecular orbitals. The elements of the Kohn-Sham matrix F^{σ} can generally be written as

$$F^{\sigma}_{pq} = h^{\sigma}_{pq} + \sum_{i\sigma'}(p_\sigma q_\sigma|i_{\sigma'}i_{\sigma'}) + (p_\sigma|v^{\sigma}_{\mathrm{XC}}|q_\sigma) - \sum_{i\sigma'}(p_\sigma i_{\sigma'}|k_X|i_{\sigma'}q_\sigma) \tag{4}$$

under the Mulliken notation for the integrals. The first term h includes both the kinetic energy operator and the nuclear attraction, while the third term v^{σ}_{XC} is the XC potential for spin σ. The last term in Eq. (4) represents the contribution from HF exchange

$$(p_\sigma q_\sigma|k_X|r_{\tau'}s_\tau) = c_X(p_\sigma q_\sigma|r_{\tau'}s_\tau) + c^{\mathrm{LR}}_X(p_\sigma q_\sigma|r_{\tau'}s_\tau)_\mu, \tag{5}$$

where the parameters c_X and c^{LR}_X depend on the chosen functional. The first term in Eq. (5) refers to the global hybrid (GH), while the second term refers to the range-separated hybrid (RSH) functional with the long-range part of the attenuated integral

$$(p_\sigma q_{\sigma'}|r_{\tau'}s_\tau)_\mu = (p_\sigma q_{\sigma'}|\frac{\mathrm{erf}(\mu r_{12})}{r_{12}}|r_{\tau'}s_\tau). \tag{6}$$

The elements of the coupling matrix $K^{\sigma\tau,\sigma'\tau'}$ in Eq. (2) can generally be written as

$$[K^{\sigma\tau,\sigma'\tau'}]_{pq,rs} = (p_\sigma q_\tau|s_{\tau'}r_{\sigma'}) + [K^{\sigma\tau,\sigma'\tau'}_{\mathrm{XC}}]_{pq,rs} - (p_\sigma r_{\sigma'}|k_X|s_{\tau'}q_\tau), \tag{7}$$

the second term of which arises from the pure density functional contribution. Under the adiabatic approximation, the matrix elements of the XC kernel take the following form:

$$[K^{\sigma\sigma,\tau\tau}_{\mathrm{XC}}]_{pq,rs} = \iint \psi_{p\sigma}(\mathbf{r})\psi_{q\sigma}(\mathbf{r}) \times \frac{\delta v^{\sigma}_{\mathrm{XC}}(\mathbf{r})}{\delta\rho_\tau(\mathbf{r}')}\Big|_{(\rho_0,\nabla\rho_0)} \psi_{s\tau}(\mathbf{r}')\psi_{r\tau}(\mathbf{r}')d\mathbf{r}d\mathbf{r}' \tag{8}$$

for spin-conserving excitations ($\Delta M_s = 0$), and the following form:[6]

$$[K_{\rm XC}^{\sigma\bar{\sigma},\sigma\bar{\sigma}}]_{pq,rs} = \int \psi_{p\sigma}(\mathbf{r})\psi_{q\bar{\sigma}}(\mathbf{r}) f_{\rm XC}^{\sigma\bar{\sigma}}(\mathbf{r})\psi_{s\bar{\sigma}}(\mathbf{r})\psi_{r\sigma}(\mathbf{r})d\mathbf{r},$$

$$f_{\rm XC}^{\sigma\bar{\sigma}}(\mathbf{r}) = \frac{v_{\rm XC}^{\sigma}(\mathbf{r}) - v_{\rm XC}^{\bar{\sigma}}(\mathbf{r})}{\rho_\sigma(\mathbf{r}) - \rho_{\bar{\sigma}}(\mathbf{r})}\Big|_{(\rho_0,\nabla\rho_0)} \quad \bar{\sigma} \neq \sigma \tag{9}$$

for spin-flip excitations ($\Delta M_s = \pm 1$). It is hence clear that the **A** and **B** matrices have the following structure:

$$\mathbf{A} = \begin{bmatrix} \mathbf{A}^{\alpha\alpha,\alpha\alpha} & \mathbf{A}^{\alpha\alpha,\beta\beta} \\ \mathbf{A}^{\beta\beta,\alpha\alpha} & \mathbf{A}^{\beta\beta,\beta\beta} \end{bmatrix}, \quad \mathbf{B} = \begin{bmatrix} \mathbf{B}^{\alpha\alpha,\alpha\alpha} & \mathbf{B}^{\alpha\alpha,\beta\beta} \\ \mathbf{B}^{\beta\beta,\alpha\alpha} & \mathbf{B}^{\beta\beta,\beta\beta} \end{bmatrix} \tag{10}$$

for spin-conserving excitations, and the following structure:

$$\mathbf{A} = \begin{bmatrix} \mathbf{A}^{\alpha\beta,\alpha\beta} & \mathbf{0} \\ \mathbf{0} & \mathbf{A}^{\beta\alpha,\beta\alpha} \end{bmatrix}, \quad \mathbf{B} = \begin{bmatrix} \mathbf{0} & \mathbf{B}^{\alpha\beta,\beta\alpha} \\ \mathbf{B}^{\beta\alpha,\alpha\beta} & \mathbf{0} \end{bmatrix} \tag{11}$$

for spin-flip excitations. The respective eigenvectors for flip-up and flip-down excitations are then structured as

$$(\mathbf{X}_I^{\alpha\beta}, \mathbf{0}, \mathbf{0}, \mathbf{Y}_I^{\beta\alpha})^T, \quad (\mathbf{0}, \mathbf{X}_I^{\beta\alpha}, \mathbf{Y}_I^{\alpha\beta}, \mathbf{0})^T. \tag{12}$$

To expedite the computation, Eq. (1) can be rewritten as a non-Hermitian eigenvalue problem of halved dimension

$$(\mathbf{A} - \mathbf{B})(\mathbf{A} + \mathbf{B})\mathbf{Z} = \omega^2\mathbf{Z}, \quad \mathbf{Z} = \mathbf{X} + \mathbf{Y}, \tag{13}$$

which can be solved efficiently by using the modified Davidson iterative scheme.[19] Since the Kohn-Sham ground state is already correlated, the effect of the **B** term for de-excitations is usually very small. Setting $\mathbf{B} = 0$ in Eq. (1) then leads to the TDA: (Ref. 20)

$$\mathbf{AX} = \omega\mathbf{X}. \tag{14}$$

It is seen from Eq. (11) that the TDA flip-up and flip-down excitations are decoupled, meaning that they can be treated separately. Compared with the full TD-DFT, TDA is not only very accurate but also is immune to the so-called (near) instability problem due to the decoupling of excitations and de-excitations. In particular, when the calculated excitation energies are rather small, the energy gradients of TDA remain finite but those of TD-DFT may approach infinity.[21] Therefore, SF-TDA is particularly suited for studying global potential energy surfaces.

III. IMPLEMENTATION AND COMPUTATIONAL DETAILS

The full noncollinear hybrid kernel has already been defined in Eq. (7). Yet, the contribution from the pure density functionals requires further elaboration. The GGA potential $v_{\rm XC}^{\sigma}$ in Eq. (9) can be handled in two different ways. One is to directly evaluate the potential as

$$v_{\rm XC}^{\sigma} = \frac{\partial e_{\rm XC}}{\partial \rho_\sigma} - \nabla \cdot \frac{\partial e_{\rm XC}}{\partial \nabla \rho_\sigma} = \frac{\partial e_{\rm XC}}{\partial \rho_\sigma} - \nabla \cdot \left(2\frac{\partial e_{\rm XC}}{\partial \gamma_{\sigma\sigma}}\nabla\rho_\sigma + \frac{\partial e_{\rm XC}}{\partial \gamma_{\sigma\bar{\sigma}}}\nabla\rho_{\bar{\sigma}} \right) \tag{15}$$

with $e_{\rm XC}$ being the XC energy density of the GGA functional

$$E_{\rm XC} = \int e_{\rm XC}(\rho_\alpha, \rho_\beta, \gamma_{\alpha\alpha}, \gamma_{\alpha\beta}, \gamma_{\beta\beta})dV,$$
$$\gamma_{\sigma\tau} = \nabla\rho_\sigma \cdot \nabla\rho_\tau. \tag{16}$$

More detailed expressions for $v_{\rm XC}^{\sigma}$ can be found from Appendix A 1. Both the first and second order derivatives of the basis functions are required here. However, once $v_{\rm XC}^{\sigma}$ is constructed, the subsequent TD-DFT calculations are the same for GGA and LDA. Alternatively, the "integration by part" can be performed when evaluating the matrix elements of $K_{\rm XC}^{\sigma\bar{\sigma},\sigma\bar{\sigma}}$ (see Appendix A 2). This scheme requires only the first order derivatives of the basis functions. Yet, the subsequent TD-DFT calculations are more expensive with GGA than with LDA. In addition, the terms involving $(\rho_\sigma - \rho_{\bar{\sigma}})^{-2}$ may become numerically instable when $\rho_\sigma \approx \rho_{\bar{\sigma}}$ at some grid points. Both schemes have been implemented here for the GGA, GH, and RSH functionals although it is the former that is actually preferred.

Some approximations to the full XC kernel equation (7) are possible to reduce the computational cost. The simplest choice is ALDA. However, such an approximation is only useful for pure density functionals. For GH functionals, the contribution (c_X) of HF exchange should always be retained even though the pure functional part can still be replaced with ALDA scaled by $(1 - c_X)$. This *ansatz* has been termed ALDAh.[22] However, it cannot be applied to RSH functionals, where the amount of HF exchange varies with inter-electronic distances. To cover all these cases we propose here a different approximation in the spirit of ALDA. That is, the density gradients $\nabla\rho_\sigma$ in $v_{\rm XC}^{\sigma}$, Eq. (15), are all set to zero, such that $v_{\rm XC}^{\sigma}$ is reduced simply to $(\partial e_{\rm XC}/\partial\rho_\sigma)|_{(\rho_\sigma,\rho_{\bar{\sigma}},0,0,0)}$. This approximation is to be dubbed as ALDA0 for it retains only the LDA part of the GGA contribution to the kernel. For instance, the short-range Becke88 exchange in CAM-B3LYP (Ref. 23) is reduced to the short-range Slater exchange. Note that, for GGA functionals (e.g., LYP (Ref. 24)) not in the form of LDA multiplied by an enhancement factor, ALDA0 is different from ALDA in the absence of HF exchange and also different from ALDAh in the presence of HF exchange. Note in passing that the collinear XC kernel can be regarded as a further approximation to ALDA0 by neglecting the entire term of Eq. (9).

Actually, ALDA0 is not merely an approximation for computational ease, but also an effective means to avoid numerical instabilities associated with the noncollinear GGA kernel, which are often encountered in describing CV types of spin-flip excitations of open-shell systems. This can be understood in view of Eq. (9): If $\rho_\alpha(\mathbf{r}_g)$ is close to $\rho_\beta(\mathbf{r}_g)$ but $\nabla\rho_\alpha(\mathbf{r}_g)$ is still significantly different from $\nabla\rho_\beta(\mathbf{r}_g)$ at a given grid point $\mathbf{r}_g$, the GGA kernel $f_{\rm XC}^{\alpha\beta}(\mathbf{r}_g)$ $(= f_{\rm XC}^{\beta\alpha}(\mathbf{r}_g))$ will be extremely large. If both excitations pq and rs involve open-shell orbitals, the singularity will be smeared out, since every

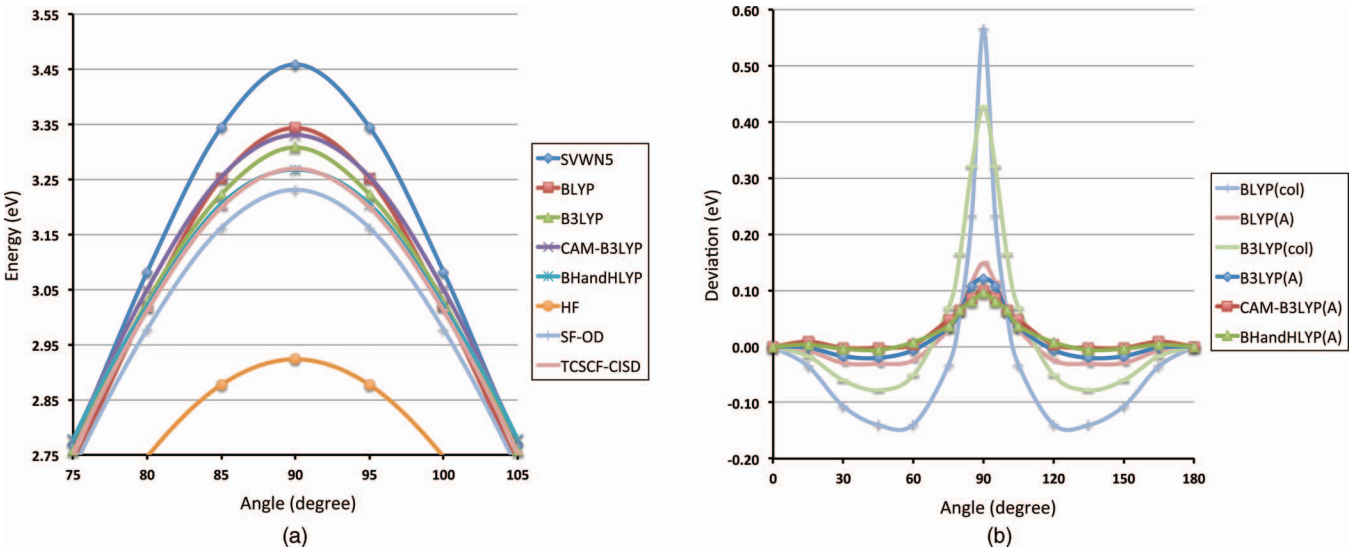

FIG. 1. Potential energy curves of the ethylene torsion: (a) SF-TDA with full noncollinear kernels, to be compared with SF-OD (Ref. 33) and TCSCF-CISD.(Ref. 38) All the curves are aligned at the same planar equilibrium. (b) Deviations of SF-TDA(col)[1] and SF-TDA(A) from SF-TDA.

open-shell orbital must also be close to zero at point $\mathbf{r}_g$, in view of the relation $\rho_\alpha(\mathbf{r}_g) - \rho_\beta(\mathbf{r}_g) \cong \sum_{p\in O} |\psi_p(\mathbf{r}_g)|^2$ (the equality holds for restricted open-shell Kohn-Sham (ROKS) orbitals) and the assumption $\rho_\alpha(\mathbf{r}_g) \approx \rho_\beta(\mathbf{r}_g)$. However, if the excitations pq and rs are of CV($\beta\alpha$) or CV($\alpha\beta$) type, the singularity in the kernel $f_{\mathrm{XC}}^{\alpha\beta}(\mathbf{r}_g)$ cannot be canceled out, since the values of closed- and vacant-shell orbitals are not necessarily small at $\mathbf{r}_g$. As a result, the GGA couplings $[K_{\mathrm{XC}}^{\sigma\bar{\sigma},\sigma\bar{\sigma}}]_{pq,rs}$ of Eq. (9) may give rise to unphysical results for CV($\beta\alpha$) and CV($\alpha\beta$) types of excitations. Even the OO($\alpha\beta$) type of excitations may be affected indirectly by such instabilities, for the flip-up and flip-down excitations are fully coupled in SF-TD-DFT. This defect can be cured by ALDA0, where both $\nabla\rho_\alpha(\mathbf{r})$ and $\nabla\rho_\beta(\mathbf{r})$ are set to zero. In particular, if $\rho_\sigma = \rho_{\bar{\sigma}}$ at point $\mathbf{r}_g$, the following relation[5] can be used for the ALDA0 kernel:

$$\left[\frac{\frac{\partial e_{\mathrm{XC}}}{\partial\rho_\sigma} - \frac{\partial e_{\mathrm{XC}}}{\partial\rho_{\bar{\sigma}}}}{\rho_\sigma - \rho_{\bar{\sigma}}}\right]_{\rho_\sigma=\rho_{\bar{\sigma}}} = \left[\frac{\partial^2 e_{\mathrm{XC}}}{\partial\rho_\sigma^2} - \frac{\partial^2 e_{\mathrm{XC}}}{\partial\rho_\sigma\partial\rho_{\bar{\sigma}}}\right]_{\rho_\sigma=\rho_{\bar{\sigma}}}, \quad (17)$$

where the right hand side is obtained from the Taylor expansion of the left hand side. Alternatively, the defect can also be removed by retaining only the leading term (i.e., $v_{\mathrm{XC}}^{\sigma}|_{(\rho_\sigma,\rho_{\bar{\sigma}},\gamma_C,\gamma_C,\gamma_C)}$) in the Taylor expansion of v_{XC}^{σ} at the point $(\rho_\sigma, \rho_{\bar{\sigma}}, \gamma_C, \gamma_C, \gamma_C)$, where $\gamma_C = (1/4)(\gamma_{\sigma\sigma} + 2\gamma_{\sigma\bar{\sigma}} + \gamma_{\bar{\sigma}\bar{\sigma}})$. This amounts to neglecting only the spin density gradients but retaining the total density gradient. However, in practice, this approximation does not seem to be better than the much simpler ALDA0. Therefore, it is not further investigated here.

All the calculations are performed with the Gaussian-based DFT and TD-DFT modules[5,18] in the in-house BDF package.[25–28] The employed XC functionals include SVWN5,[29] BLYP,[24,30] B3LYP,[31,32] BHandHLYP,[24,30,31] CAM-B3LYP,[23] and pure HF, which are featured by an increased amount of long-range exact exchange. Both the ALDA0 and the full noncollinear XC kernels are used for spin-flip excitations. The former will be denoted as SF-TD-DFT(A) or SF-TDA(A). In the case of pure HF, the notation SF-RPA (random phase approximation) or SF-CIS (Ref. 33) (configuration interaction with singles) would be the equivalent of SF-TD-DFT or SF-TDA. For comparison, some benchmark MRCISD+Q (multi-reference configuration interaction with singles and doubles plus the Davidson correction) calculations are also carried out with the Xi'an-CI module[34–36] interfaced into the BDF package.

IV. RESULTS AND DISCUSSION

A. Ethylene torsion

The twisted ethylene is one of the classic examples with strong non-dynamical correlation. The π^2 configuration dominates at the planar equilibrium (R(CC) = 1.330 Å, R(CH) = 1.076 Å, ∠(HCH) = 116.6°),[33] whereas the π^2 and $(\pi^*)^2$ configurations become equally important when the dihedral angle θ between the two methylene planes is increased to 90°. Therefore, a spin-conserving single reference description is qualitatively correct at $\theta = 0°$ but becomes progressively deteriorated as the dihedral angle increases. For instance, both the KS and HF PECs have an unphysical cusp at $\theta = 90°$ companied by a too high barrier.[1] As seen from Fig. 1(a), the situation is much improved by SF-TDA combined with the noncollinear functionals (SVWN5, BLYP, B3LYP, BHandHLYP, and CAM-B3LYP): All the PECs calculated with the high-spin unrestricted KS (UKS) reference $(\pi\alpha)(\pi^*\alpha)$ and the DZP basis sets[37] are smooth around $\theta = 90°$. The barrier height tends to decrease as the amount of HF exchange increases and eventually becomes too low for pure HF (i.e., SF-CIS). In particular, the BHandHLYP curve almost coincides with the TCSCF-CISD (configuration interaction with singles and doubles using two-configuration self-consistent-field orbitals) curve,[38] and deviates only marginally from the SF-OD (coupled-cluster doubles based on optimized orbitals) one.[33] To reveal the effect of the XC kernel, the SF-TDA PECs with the approximate and full XC kernels are further compared in Fig. 1(b). It is first seen that the PEC by the collinear BLYP

TABLE I. Energies (in eV) of ethylene calculated by SF-TD-DFT (SF-RPA) and SF-TDA (SF-CIS) with the high-spin UKS (UHF) reference $(\pi\alpha)(\pi^*\alpha)$ at the equilibrium ($\theta = 0^\circ$) and distorted ($\theta = 90^\circ$) geometries. $\Delta E_{\rm ref} = E_{\rm ref}(90^\circ) - E_{\rm ref}(0^\circ)$; $\omega_{\rm gs}(\theta)$: vertical de-excitation energy of the ground state; $\Delta\omega = \omega_{\rm gs}(90^\circ) - \omega_{\rm gs}(0^\circ)$; ΔE: barrier height ($=\Delta E_{\rm ref} + \Delta\omega$). ROKS-based results are in parentheses.

Functional	Method	$\Delta E_{\rm ref}$	$\omega_{\rm gs}(0^\circ)$	$\delta\omega_1$[a]	$\delta\omega_2$[b]	$\omega_{\rm gs}(90^\circ)$	$\delta\omega_1$[a]	$\delta\omega_2$[b]	$\Delta\omega$	$\delta\omega_1$[a]	$\delta\omega_2$[b]	ΔE
SVWN5	TD-DFT	−1.55 (−1.57)	−4.92 (−5.00)			0.06 (−0.02)			4.98 (4.98)			3.43 (3.41)
	TDA	−1.55 (−1.57)	−4.88 (−4.96)	0.04		0.12 (0.09)	0.06		5.01 (5.05)	0.03		3.46 (3.48)
BLYP	TD-DFT	−1.44 (−1.46)	−4.72 (−4.83)			0.03 (−0.02)			4.75 (4.80)			3.31 (3.35)
	TDA	−1.44 (−1.46)	−4.68 (−4.79)	0.05		0.10 (0.04)	0.08		4.78 (4.83)	0.03		3.34 (3.37)
	TD-DFT(A)	−1.44 (− 1.46)	−4.34 (−4.46)		0.38	0.57 (0.49)		0.54	4.91 (4.95)		0.16	3.47 (3.49)
	TDA(A)	−1.44 (−1.46)	−4.31 (−4.43)	0.03	0.37	0.62 (0.49)	0.05	0.52	4.93 (4.92)	0.02	0.15	3.49 (3.46)
B3LYP	TD-DFT	−1.38 (−1.40)	−4.67 (−4.78)			− 0.03 (−0.07)			4.63 (4.71)			3.25 (3.31)
	TDA	−1.38 (−1.40)	−4.60 (−4.73)	0.07		0.08 (0.02)	0.12		4.68 (4.75)	0.05		3.31 (3.35)
	TD-DFT(A)	−1.38 (−1.40)	−4.36 (−4.51)		0.30	0.41 (0.31)		0.44	4.77 (4.81)		0.14	3.39 (3.41)
	TDA(A)	−1.38 (−1.40)	−4.32 (−4.46)	0.04	0.28	0.49 (0.39)	0.08	0.40	4.81 (4.85)	0.04	0.12	3.43 (3.45)
BHandHLYP	TD-DFT	−1.30 (−1.32)	−4.58 (−4.74)			− 0.08 (−0.16)			4.50 (4.58)			3.20 (3.26)
	TDA	−1.30 (−1.32)	−4.49 (−4.66)	0.10		0.08 (−0.03)	0.17		4.57 (4.63)	0.07		3.27 (3.31)
	TD-DFT(A)	−1.30 (−1.32)	−4.33 (−4.52)		0.25	0.27 (0.12)		0.36	4.60 (4.64)		0.10	3.31 (3.32)
	TDA(A)	−1.30 (−1.32)	−4.26 (−4.44)	0.07	0.23	0.40 (0.26)	0.13	0.32	4.66 (4.70)	0.06	0.10	3.36 (3.38)
CAM-B3LYP	TD-DFT	−1.35 (−1.37)	−4.76 (−4.91)			− 0.21 (−0.28)			4.55 (4.63)			3.20 (3.26)
	TDA	−1.35 (−1.37)	−4.60 (−4.74)	0.17		0.09 (0.01)	0.30		4.68 (4.74)	0.13		3.33 (3.37)
	TD-DFT(A)	−1.35 (−1.37)	−4.56 (−4.71)		0.20	0.08 (−0.03)		0.29	4.65 (4.68)		0.09	3.29 (3.31)
	TDA(A)	−1.35 (−1.37)	−4.39 (−4.53)	0.17	0.21	0.39 (0.29)	0.31	0.31	4.78 (4.82)	0.14	0.10	3.43 (3.45)
HF	RPA	−1.11 (−1.16)	−4.14 (−4.56)			− 0.26 (−0.56)			3.89 (4.00)			2.78 (2.84)
	CIS	−1.11 (−1.16)	−3.92 (−4.30)	0.23		0.11 (−0.16)	0.37		4.03 (4.14)	0.14		2.92 (2.98)
Difference[c]		−0.02	−0.13			−0.09			0.04			0.02

[a]Difference between TDA and TD-DFT.
[b]Difference between the ALDA0 and the full kernels.
[c]Mean difference between ROKS- and UKS-based results.

kernel has a cute cusp alongside with a too high barrier of 3.91 eV.[1] This is a direct consequence of missing the coupling between the $\pi\alpha \rightarrow \pi^*\beta$ and $\pi^*\alpha \rightarrow \pi\beta$ transitions. Such coupling is partly taken into account by mixing in some HF exchange in the functional, such that even the collinear SF-TDA/B3LYP curve shows no cusp. However, the barrier (3.74 eV) (Ref. 1) is still too high as compared with the TCSCF-CISD value of 3.27 eV (Ref. 38) or the SF-OD value of 3.23 eV.[33] The real improvement stems from the noncollinear XC kernel by which the above coupling is fully accounted for: The barriers by the full noncollinear SF-TDA/BLYP (3.34 eV) and SF-TDA/B3LYP (3.31 eV) are both very close to the TCSCF-CISD and SF-OD values. They are only slightly worsened by the ALDA0 approximation for the XC kernel, leading to 3.49 and 3.43 eV for the BLYP and B3LYP functionals, respectively (see Table I).

Having briefly discussed the general features of the PECs, we turn to the comparison between SF-TD-DFT and SF-TDA combined with the various XC functionals and kernels. The calculated vertical de-excitation energies $\omega_{\rm gs}(\theta)$ of the singlet ground state from the UKS reference $(\pi\alpha)(\pi^*\alpha)$ are given in Table I for the two extreme geometries with $\theta = 0^\circ$ and $\theta = 90^\circ$. Together with the differential reference energy $\Delta E_{\rm ref}$, the unoptimized barrier height ΔE has been derived. Note in passing that such UKS-based results are very close to the ROKS-based ones. Overall, the SF-TDA results for $\omega_{\rm gs}(\theta)$ and hence ΔE deviate very little from the SF-TD-DFT values. However, the deviations tend to increase as the amount of HF exchange increases. This is not surprising as the **B** term becomes more effective for functionals with more nonlocal exchange. In the limit case of pure HF, the deviation of SF-CIS from SF-RPA becomes largest, up to 0.4 eV for $\omega_{\rm gs}(90^\circ)$. The errors introduced by the ALDA0 approximation to the full kernel are grossly larger than those introduced by TDA to TD-DFT, and the trends of the errors are also different. The ALDA0 errors actually decrease as the amount of HF exchange increases. It is again not surprising as the approximation becomes naturally smaller if the parent pure density functional itself has a smaller weight in the kernel. As a result, the TDA and ALDA0 errors become comparable for BHandHLYP and CAM-B3LYP. Although the individual errors for $\omega_{\rm gs}(\theta)$ introduced by both approximations vary between 0.3 and 0.6 eV, the relative energies $\Delta\omega$ ($=\omega_{\rm gs}(90^\circ) - \omega_{\rm gs}(0^\circ)$) predicted by SF-TDA(A) deviate from the full SF-TD-DFT values by only ∼0.2 eV for all the functionals.

To see whether the degeneracy of a spin multiplet is conserved or not, the energy difference $\omega_{\rm ref}(\theta)$ between the $M_s = 0$ and $M_s = 1$ components of the triplet reference is given in Table II for each geometry. The numerical degeneracy (i.e., $\omega_{\rm ref}(\theta) = 0$) achieved by the full UKS/SF-TD-DFT (and UHF/SF-RPA) has come out as a big surprise, since neither the reference nor the excitation manifold is spin-adapted. This provokes us to think of a formal proof. As shown in Appendix B 1, the degeneracy indeed holds strictly, not by chance. As a matter of fact, it is the Brillouin condition that guarantees such spin degeneracy. A close inspection then reveals that the small lift of the degeneracy by UKS/SF-TD-DFT/CAM-B3LYP is factually due to weak numerical instabilities in the presence of CV types of excitations. In contrast, the use of ROKS orbitals in SF-TD-DFT calculations does

TABLE II. UKS (UHF)-based SF-TD-DFT (SF-RPA) and SF-TDA (SF-CIS) calculations of the energetic separations ($\omega_{\text{ref}}(\theta)$ in eV) between the $M_s = 0$ and $M_s = 1$ components of the triplet reference of ethylene at the equilibrium ($\theta = 0^\circ$) and distorted ($\theta = 90^\circ$) geometries. ROKS-based results are in parentheses.

Functional	Method	$\omega_{\text{ref}}(0^\circ)$	$\delta\omega_1$[a]	$\delta\omega_2$[b]	$\omega_{\text{ref}}(90^\circ)$	$\delta\omega_1$[a]	$\delta\omega_2$[b]
SVWN5	TD-DFT	0.00 (−0.08)			0.00 (−0.04)		
	TDA	0.04 (−0.03)	0.04		0.02 (−0.02)	0.02	
BLYP	TD-DFT	0.00 (−0.09)			0.00 (−0.07)		
	TDA	0.06 (−0.05)	0.06		0.04 (−0.03)	0.04	
	TD-DFT(A)	0.65 (0.52)		0.65	0.51 (0.43)		0.51
	TDA(A)	0.68 (0.56)	0.03	0.62	0.53 (0.45)	0.02	0.49
B3LYP	TD-DFT	0.00 (−0.11)			0.00 (−0.09)		
	TDA	0.07 (−0.06)	0.07		0.05 (−0.04)	0.05	
	TD-DFT(A)	0.49 (0.34)		0.49	0.40 (0.30)		0.40
	TDA(A)	0.53 (0.39)	0.04	0.46	0.43 (0.33)	0.03	0.38
BHandHLYP	TD-DFT	0.00 (−0.16)			0.00 (−0.13)		
	TDA	0.10 (−0.08)	0.10		0.07 (−0.06)	0.07	
	TD-DFT(A)	0.38 (0.19)		0.38	0.33 (0.18)		0.33
	TDA(A)	0.45 (0.27)	0.07	0.35	0.38 (0.24)	0.05	0.31
CAM-B3LYP	TD-DFT	− 0.14 (−0.24)			− 0.10 (−0.19)		
	TDA	0.07 (−0.06)	0.21		0.04 (−0.04)	0.14	
	TD-DFT(A)	0.25 (0.10)		0.39	0.23 (0.12)		0.33
	TDA(A)	0.42 (0.28)	0.17	0.35	0.34 (0.24)	0.11	0.30
HF	RPA	0.00 (−0.41)			0.00 (−0.30)		
	CIS	0.20 (−0.17)	0.20		0.14 (−0.13)	0.14	
Difference[c]		−0.13			−0.09		

[a]Difference between TDA and TD-DFT.
[b]Difference between the ALDA0 and the full kernels.
[c]Mean difference between ROKS- and UKS-based results.

lead to real breaking of the degeneracy, which can only be avoided by excluding all the CV types of excitations (see Appendix B 2). Otherwise, the $M_s = 0$ component is always lower in energy than the $M_s = 1$ component. The more so, the more HF exchange in the functional, see Table II. The situation is very much the same as the energy $\omega_{\text{gs}}(\theta)$ of the ground state: The ROKS/SF-TD-DFT value is also lower by a similar amount than the UKS/SF-TD-DFT one. These findings dictate that only the combination of UKS with SF-TD-DFT and that of ROKS with spin-adapted SF-TD-DFT (Refs. 4 and 5) are internally consistent. It is worth noting that the degeneracy is violated only slightly by UKS/SF-TDA but strongly by ALDA0. The latter amounts to 0.65 eV for BLYP but becomes progressively smaller to 0.20 eV for pure HF. It is also noticeable that the ALDA0 errors for $\omega_{\text{ref}}(\theta)$ are somewhat larger than those for $\omega_{\text{gs}}(\theta)$ (see Table I), especially with BLYP and B3LYP. This is because the magnitude of any approximation to Eq. (9) would depend on the degree of overlap between the transition pairs: The larger the overlap, the larger the error.

Although SF-TD-DFT with the full XC kernel is more consistent than the SF-TDA variant, it is not really recommended for studying global PECs for two reasons. First, if the target states are to be accessed by de-excitations ($\omega < 0$), they are not necessarily the lowest roots of Eq. (13), since Eq. (13) gives arise to ω^2 instead of ω such that excited states of positive excitation energies smaller than $|\omega|$ are lower than the target states in the spectrum of Eq. (13). This will make the identification of the target states difficult. In contrast, they will always be the lowest roots of Eq. (14). Second, as already mentioned before, the SF-TD-DFT energy may become totally unreliable when the (near) instability appears in the reference state at some geometry. Therefore, it is SF-TDA that is preferred for studying global PECs. Furthermore, SF-TDA has to be combined with ALDA0 for general cases (vide post) to avoid the aforementioned numerical instabilities associated with the noncollinear GGA kernel. As shown before, SF-TDA(A) is indeed fairly accurate for relative energies.

B. C_{2v} ring-opening of oxirane

To further confirm the previous findings, we now consider the ring-opening reaction of oxirane, which is another difficult example for single reference approaches. Around the avoided crossing ($\angle(\text{COC}) \approx 120^\circ$) on the C_{2v} ring-opening pathway, the occupied $6a_1\,(\sigma)$ and unoccupied $4b_2\,(\sigma^*)$ orbitals become quasi-degenerate, leading to a cusp in the SC-TD-DFT energy profile for the 2^1A_1 state.[39] It was shown[13] recently that the cusp can be removed by SF-TDA/SVWN5. However, the SF-TDA/SVWN5 energy profile is correct only qualitatively but not quantitatively: The error is still as large as 2 eV around the avoided crossing. This motivates the present study with more refined functionals. The same geometry and 6-311++G(2*d*,2*p*) basis sets[40] are used as in Ref. 13. The 1^3B_2 state of configuration $(6a_1\alpha)(4b_2\alpha)$ is taken as the reference. The present SF-TDA and SF-TDA(A) and the previous QMC (quantum Monte Carlo)[39] energy profiles are plotted in Fig. 2 for the 1^1A_1, 1^3B_2, and 2^1A_1 states. One main message here is that the effect of HF exchange is crucial for describing the avoided crossing at $\angle(\text{COC}) \approx 120^\circ$. At this point the energy of 2^1A_1 is underestimated by ∼2 eV by SF-TDA/SVWN5 (and BLYP) but overestimated by ∼1.5 eV by SF-TDA/HF (i.e., SF-CIS). The results by the B3LYP,

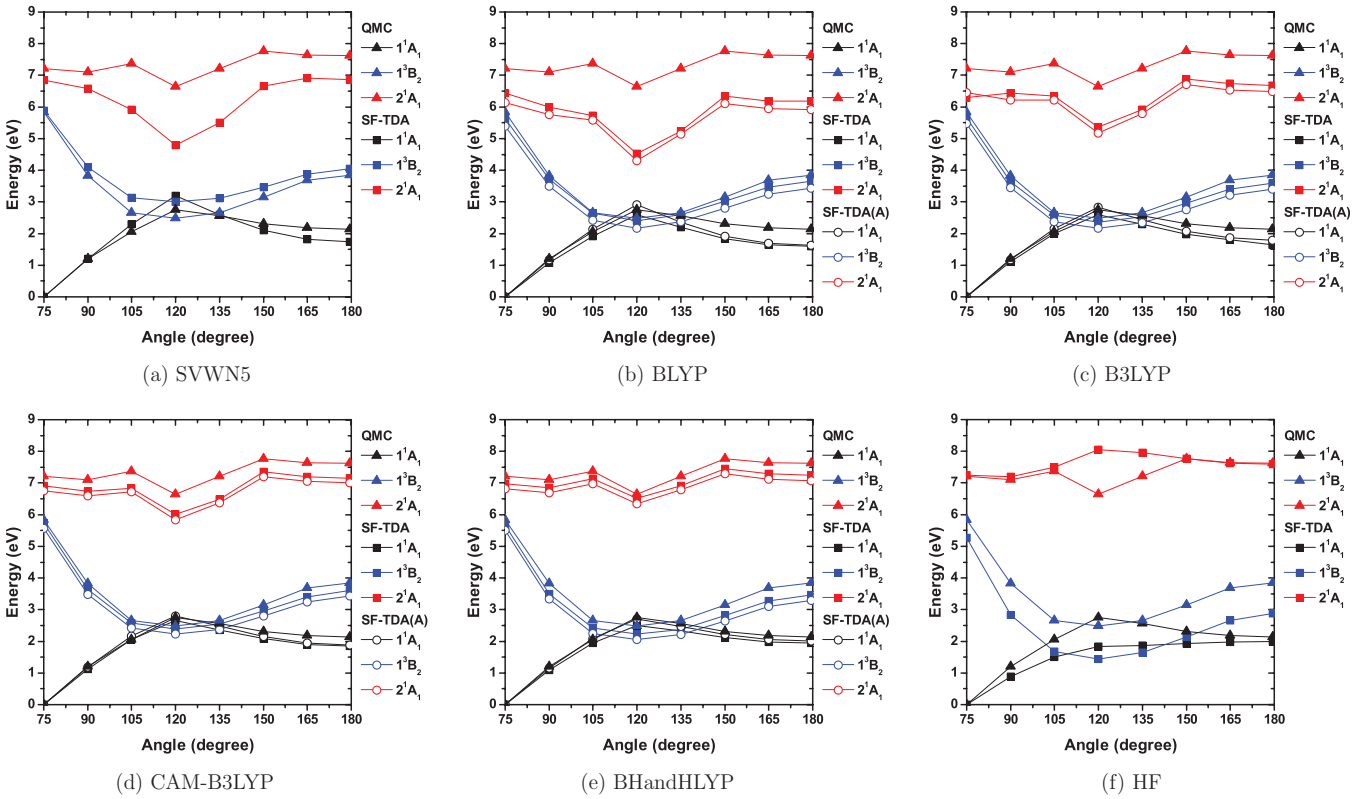

FIG. 2. SF-TDA, SF-TDA(A), and QMC energy profiles for the 1^1A_1, 1^3B_2, and 2^1A_1 states of oxirane along the C_{2v} ring-opening pathway. All the curves are aligned at the ring-opening angle of 75°.

CAM-B3LYP, and BHandHLYP functionals lie in between and are grossly in good agreement with the QMC results. Especially, the deviations of BHandHLYP from QMC are within 0.5 eV along the whole reaction pathway. This is similar to the ethylene torsion, where the barrier height is well reproduced by the GH and RSH functionals but is overestimated by SF-TDA/SVWN5 (and BLYP) and underestimated by SF-CIS.

As pointed out before, SF-TDA (and SF-TD-DFT) with the full noncollinear kernel may suffer from numerical instabilities. It is indeed observed here: SF-TDA sometimes gives rise to large negative excitation energies for some CV($\alpha\beta$) transitions. In this case, the 1^1A_1 and 2^1A_1 states have to be identified carefully, e.g., by examining their compositions. Alternatively, a different set of grid points other than that used in the ground state calculation has to be chosen for the excited state calculation. In contrast, SF-TDA(A) is immune to such instabilities. It is seen from Fig. 2 that the SF-TDA(A) curves do parallel closely the SF-TDA ones. Therefore, SF-TDA(A) as a combination of SF-TDA and ALDA0 is highly recommended for investigating properties of global PECs.

C. Spin multiplet states of closed-shell systems

For a well-behaved closed-shell system, the $M_s = 0$ component of the lowest triplet state can be accessed by SC-TD-DFT through spin-conserving single excitation from the ground state. Reversely, the ground state can be accessed by SF-TD-DFT through flip-down de-excitation from the $M_s = 1$ component of the triplet. The so-obtained absolute energies are to be denoted as ω_T^{SC} and ω_T^{SF}, respectively. On the other hand, the energy difference $\omega_T^{\Delta SCF}$ between the triplet state and the ground state can also be calculated variationally through the self-consistent-field (SCF) procedure (ΔSCF). The singlet excited state sharing the same configuration with the triplet state can also be obtained from both SC-TD-DFT and SF-TD-DFT. The respective singlet-triplet gaps are to be denoted as $\Delta\omega_{ST}^{SC}$ and $\Delta\omega_{ST}^{SF}$. Ideally, the identities $\omega_T^{SC} = \omega_T^{SF} = \omega_T^{\Delta SCF}$ and $\Delta\omega_{ST}^{SC} = \Delta\omega_{ST}^{SF}$ should hold exactly. However, with approximate XC functionals, these quantities calculated by SC-TD-DFT, SF-TD-DFT, and ΔSCF can be very different, as shown by Wang and Ziegler[7] in their calculations of H_2O, CH_2O, and C_2H_4 with the SVWN5 functional. To gain deeper insights, these quantities for the same molecules are recalculated with SC-TDA, UKS-based SF-TDA, and SF-TDA(A) in conjunction with the SVWN5, BLYP, B3LYP, CAM-B3LYP, BHandHLYP, and pure HF functionals and the aug-cc-pVTZ basis sets.[41] The results are collected in Table III. The geometries are taken from Ref. 20 and the experimental results are taken from Refs. 42–44.

The previous findings[7] with the SVWN5 functional are indeed confirmed here: For the $^3B_1$ state of H_2O, ω_T^{SF} (8.66 eV) is significantly larger than both ω_T^{SC} (6.32 eV) and $\omega_T^{\Delta SCF}$ (7.41 eV), while for the singlet-triplet gap of C_2H_4, the difference between $\Delta\omega_{ST}^{SC}$ (3.11 eV) and $\Delta\omega_{ST}^{SF}$ (1.73 eV) amounts to 1.4 eV, much larger than the cases of H_2O (−0.14 eV) and CH_2O (0.09 eV). The overall picture is not much changed by the BLYP functional. As the amount of (short-range) HF exchange increases from BLYP though B3LYP and CAM-B3LYP to BHandHLYP, ω_T^{SC} for H_2O

TABLE III. Spin multiplet states of closed-shell molecules of H_2O, CH_2O, and C_2H_4. $\omega_T^{SC}/\omega_T^{SF}/\omega_T^{\Delta SCF}$: triplet excitation energy by SC-TDA/SF-TDA/ΔSCF; $\bar{\omega}_T = (1/2)(\omega_T^{SC} + \omega_T^{SF})$; $\Delta\omega_{ST}^{SC}/\Delta\omega_{ST}^{SF}$: singlet-triplet gap by SC-TDA/SF-TDA. The ALDA0 results are in parentheses.

Molecule	State	Method	SVWN5	BLYP	B3LYP	CAM-B3LYP	BHandHLYP	HF	Expt.[a]
H_2O	$^3B_1$	ω_T^{SC}	6.32	5.98	6.58	6.75	7.24	8.02	7.20
		Λ	0.37	0.36	0.32	0.28	0.27	0.23	
		ω_T^{SF}	8.66	8.06 (8.06)	7.57 (7.57)	7.53 (7.53)	6.73 (6.74)	4.41	
		Λ	0.38	0.39 (0.39)	0.40 (0.40)	0.42 (0.42)	0.44 (0.44)	0.50	
		$\bar{\omega}_T$	7.49	7.02	7.07	7.14	6.98	6.21	
		$\omega_T^{\Delta SCF}$	7.41	7.08	7.08	7.15	6.91	5.97	
	$^1B_1 - {}^3B_1$	$\Delta\omega_{ST}^{SC}$	0.27	0.30	0.36	0.40	0.46	0.68	0.20
		$\Delta\omega_{ST}^{SF}$	0.41	0.43 (1.10)	0.43 (0.92)	0.41 (0.83)	0.44 (0.84)	0.57	
CH_2O	$^3A_2$	ω_T^{SC}	3.05	3.14	3.23	3.23	3.39	3.71	3.50
		Λ	0.52	0.52	0.51	0.49	0.48	0.36	
		ω_T^{SF}	3.50	3.28 (3.25)	3.15 (3.12)	3.14 (3.09)	2.79 (2.76)	1.88	
		Λ	0.51	0.50 (0.50)	0.48 (0.48)	0.48 (0.48)	0.46 (0.46)	0.37	
		$\bar{\omega}_T$	3.28	3.21	3.19	3.18	3.09	2.79	
		$\omega_T^{\Delta SCF}$	3.27	3.26	3.22	3.20	3.05	2.39	
	$^1A_2 - {}^3A_2$	$\Delta\omega_{ST}^{SC}$	0.62	0.67	0.68	0.69	0.72	0.83	0.57
		$\Delta\omega_{ST}^{SF}$	0.53	0.75 (0.87)	0.54 (0.82)	0.55 (0.79)	0.54 (0.83)	0.63	
C_2H_4	$^3B_{1u}$	ω_T^{SC}	4.79	4.52	4.41	4.34	4.19	3.58	4.36
		Λ	0.88	0.87	0.83	0.75	0.73	0.62	
		ω_T^{SF}	4.82	4.60 (4.26)	4.52 (4.25)	4.54 (4.33)	4.40 (4.18)	3.78	
		Λ	0.90	0.90 (0.90)	0.90 (0.90)	0.89 (0.89)	0.88 (0.88)	0.75	
		$\bar{\omega}_T$	4.80	4.56	4.46	4.44	4.29	3.68	
		$\omega_T^{\Delta SCF}$	4.78	4.53	4.39	4.33	4.14	3.30	
	$^1B_{1u} - {}^3B_{1u}$	$\Delta\omega_{ST}^{SC}$	3.11	3.08	3.36	3.53	3.62	4.11	3.24
		$\Delta\omega_{ST}^{SF}$	1.73	1.82 (2.05)	2.23 (2.68)	3.05 (3.04)	3.61 (3.60)	5.28	

[a]Experimental data are taken from Ref. 42 for H_2O, Ref. 43 for CH_2O, and Ref. 44 for C_2H_4.

increases gradually from 5.98 eV to 7.24 eV approaching from below to the experimental value of 7.20 eV, while ω_T^{SF} decreases from 8.06 eV to 6.73 eV crossing the experimental value. In contrast, the variation of $\omega_T^{\Delta SCF}$ with respect to the functionals is only 0.2 eV. Similar patterns are also observed for CH_2O and C_2H_4. These phenomena can be understood by considering a model functional of the following form:

$$E_{XC} = c_X E_X^{HF} + (1 - c_X) E_{XC}^{DF}, \tag{18}$$

where E_X^{HF} represents the HF exchange and E_{XC}^{DF} represents the pure functional part. Assuming the same orbitals for the ground and the triplet states, the following relationships between ω_T^{SC}, ω_T^{SF}, and $\omega_T^{\Delta SCF}$ can be deduced from the single-pole approximation (SPA) to TDA:

$$\omega_T^{SC} \approx \omega_T^{\Delta SCF} - \delta\omega, \tag{19}$$

$$\omega_T^{SF} \approx \omega_T^{\Delta SCF} + \delta\omega \approx \omega_T^{SC} + 2\delta\omega, \tag{20}$$

$$\delta\omega = \frac{1}{2}(1 - c_X)(\Delta\rho | f_H + f_{XC}^{\alpha\alpha,\alpha\alpha} | \Delta\rho), \tag{21}$$

where f_H is the Coulomb kernel and $\Delta\rho = |\psi_a|^2 - |\psi_i|^2$ is the density transfer induced in the transition $\psi_i \to \psi_a$. The magnitude of $\Delta\rho$ can roughly be measured by the Λ index[45]

$$\Lambda = \sum_{ai} Z_{ai}^2 O_{ai} \in [0, 1], \quad O_{ai} = \int |\psi_a(\mathbf{r})||\psi_i(\mathbf{r})| d\mathbf{r} \tag{22}$$

under the normalization condition $\mathbf{Z}^T\mathbf{Z} = 1$. The smaller the Λ, the smaller the overlap between ψ_a and ψ_i and hence the larger $\Delta\rho$. The latter further implies larger differences between ω_T^{SC}, ω_T^{SF}, and $\omega_T^{\Delta SCF}$. A small Λ (large $\Delta\rho$) occurs usually to Rydberg (e.g., the $^3B_1$ state of H_2O with $\Lambda \approx 0.4$) or charge-transfer excitations but a large Λ (small $\Delta\rho$) occurs usually to valance excitations (e.g., the $^3B_{1u}$ state of C_2H_4 with $\Lambda \approx 0.9$). As $\delta\omega$, Eq. (21) is usually positive-valued, it is clear that, compared to ΔSCF, SC-TD-DFT tends to underestimate but SF-TD-DFT tends to overestimate by a similar amount the energy of the triplet. The average $\bar{\omega}_T$ of ω_T^{SF} and ω_T^{SC} is hence approximately equal to $\omega^{\Delta SCF}$, as verified in Table III. This may suggest a "midpoint TD-DFT," where the reference is an intermediate state with half electron in ψ_i and half electron in ψ_a.[46,47] As for the functional dependence, the difference between ω_T^{SF} and ω_T^{SC} should particularly be large for pure density functionals with $c_X = 0$ and becomes smaller as the amount c_X of exact exchange increases. In the limit of pure HF with $c_X = 1$, the difference should vanish. However, the HF orbitals of the ground and triplet states may be significantly different, such that the difference between ω_T^{SF} and ω_T^{SC} may become large again. Therefore, along the functional axis, there exists a cross point between the decreasing ω_T^{SF} and the increasing ω_T^{SC}, e.g., somewhere between CAM-B3LYP and BHandHLYP for the $^3B_1$ state of H_2O. More obvious examples are the triplet states of rare-gas atoms, which are pure Rydberg states characterized by large density transfer

$\Delta\rho$. Because of this, the energies of such states are significantly underestimated by SC-TD-DFT with pure functionals but overestimated by pure HF, whereas the reverse is true for SF-TD-DFT.[48]

The similar analysis can also be carried out for the singlet-triplet gap, for which the following relationship holds:

$$\Delta\omega_{\rm ST}^{\rm SF} = \Delta\omega_{\rm ST}^{\rm SC} - \delta\omega', \tag{23}$$

$$\delta\omega' = 2(1 - c_X)(\rho_{ai}|f_H + f_{\rm XC}^{\alpha\alpha,\alpha\alpha}|\rho_{ia}), \tag{24}$$

where $\rho_{ai} = \psi_a^*\psi_i$. Yet, opposite to the previous case, a small Λ would imply a small $\delta\omega'$ and hence a small difference between $\Delta\omega_{\rm ST}^{\rm SF}$ and $\Delta\omega_{\rm ST}^{\rm SC}$ for Rydberg or charge-transfer excitations. Accordingly, the difference between the two should be particularly large for valance excitations with a large Λ. This is indeed the case for the gap between the $^1B_{1u}$ and $^3B_{1u}$ states of C_2H_4 obtained with the SVWN5 and BLYP functionals. The difference gets reduced upon mixing in the HF exchange. Since the Λ is only $\sim$0.5 for the $^3A_2$ state of CH_2O, both the differences $\delta\omega$ and $\delta\omega'$ are not significant, as shown in Table III.

In sum, SF-TD-DFT with pure density functionals can lead to large errors for excitations with either small or large Λ. This is quite different from SC-TD-DFT, which is problematic mostly for excitations with small Λ. Only the combination of SF-TD-DFT with hybrid functionals of substantial exact exchange (e.g., CAM-B3LYP and BHandHLYP) turns out to be reliable. As noticed before, the performance of ALDA0 depends on the orbital overlaps: Typically the smaller the overlap, the better the performance. This trend is also observed here for the triplet states. However, the situation is less clear cut for the singlet-triplet gaps, as the singlet state involves two dominant transitions for which the individual ALDA0 errors may be quite different. An extreme example for this is the ALDA0 values for the $^1B_1 - {}^3B_1$ gap of H_2O, which are too large compared to the results by the corresponding full kernels.

D. Spin multiplet states of open-shell systems

In general, SC-TD-DFT that cannot obtain pure states for spatially degenerate systems for the single excitation manifold is incomplete. Typical examples are the diatomic molecules of CF, CH, and NH^+ with a $\sigma^2\pi^1$ ($^2\Pi$) ground state. The excited-state configuration $\sigma^1\pi^2$ leads to four doublets:

$$|^2\Sigma^-\rangle = \frac{1}{\sqrt{6}}(-2|\bar\sigma\pi_x\pi_y\rangle + |\sigma\pi_x\bar\pi_y\rangle + \underline{|\sigma\bar\pi_x\pi_y\rangle}), \tag{25}$$

$$|^2\Sigma^+\rangle = \frac{1}{\sqrt{2}}(|\sigma\pi_x\bar\pi_x\rangle + \underline{|\sigma\pi_y\bar\pi_y\rangle}), \tag{26}$$

$$|^2\Delta_x\rangle = \frac{1}{\sqrt{2}}(|\sigma\pi_x\bar\pi_x\rangle - \underline{|\sigma\pi_y\bar\pi_y\rangle}), \tag{27}$$

$$|^2\Delta_y\rangle = \frac{1}{\sqrt{2}}(|\sigma\pi_x\bar\pi_y\rangle - \underline{|\sigma\bar\pi_x\pi_y\rangle}), \tag{28}$$

where a barred orbital indicates a β electron. Spin-conserving single excitations from the ground state $|\sigma\bar\sigma\pi_x\rangle$ can only generate three configurations, i.e., $|\sigma\pi_x\bar\pi_x\rangle$, $|\bar\sigma\pi_x\pi_y\rangle$, and $|\sigma\pi_x\bar\pi_y\rangle$. Due to lack of the double excitations underlined in the above expressions, none of the four doublets can be described correctly. However, if the high-spin component of the quartet state $|^4\Sigma^-\rangle = |\sigma\pi_x\pi_y\rangle$ is taken as the reference, all these doublets can be accessed by flip-down single excitations. The so-obtained vertical excitation energies by SF-TDA with and without ALDA0 are given in Table IV, to be compared with the MRCI results obtained with the full valence active space. The experimental geometries,[49] the aug-cc-pVTZ basis sets,[41] and the ROKS orbitals are used here. It is seen that the energy of $|^4\Sigma^-\rangle$ is well reproduced by both SVWN5 and BLYP. However, the energies of the doublets are grossly underestimated by the pure functionals, thereby resulting in too small doublet-quartet gaps. This is again due to large overlaps between the σ and π_y orbitals ($\Lambda \approx 0.60 - 0.75$), as elucidated before for the singlet-triplet gaps of closed-shell systems. In contrast, the doublet-quartet gaps are better reproduced by the hybrid functionals (especially BHandHLYP). The ALDA0 results are within 0.15 eV agreement with the corresponding values by the full kernels.

To see to what extent the spin mulitplets can be resolved by starting with the ground state $|\sigma\bar\sigma\pi_x\rangle$, the $|^4\Sigma^-\rangle$ state is recalculated with the flip-up SF-TDA(A). Note that the full noncollinear XC kernel cannot be used for such flip-up excitations. It is seen from Table IV that the flip-up and flip-down SF-TDA(A) energies for $|^4\Sigma^-\rangle$ are close to each other only for the CAM-B3LYP and BHandHLYP functionals. The doublets are then recalculated with the spin-conserving U-TDA (unrestricted TDA; $\Delta M_s = 0$) and X-TDA (spin-adapted TDA with further RPA corrections;[18] $\Delta S = 0$). The latter can access two spin-adapted doublets through the CV type of spin-conserving excitations, viz.,

$$|D_1\rangle = \frac{1}{\sqrt{2}}(|\bar\sigma\pi_x\pi_y\rangle - |\sigma\pi_x\bar\pi_y\rangle), \tag{29}$$

$$|D_2\rangle = \frac{1}{\sqrt{6}}(-|\bar\sigma\pi_x\pi_y\rangle - |\sigma\pi_x\bar\pi_y\rangle + 2\underline{|\sigma\bar\pi_x\pi_y\rangle}). \tag{30}$$

In view of Eqs. (25) and (28), the $|^2\Sigma^-\rangle$ and $|^2\Delta_y\rangle$ states can be re-expressed as

$$|^2\Sigma^-\rangle = \frac{1}{2}(-\sqrt{3}|D_1\rangle + |D_2\rangle), \tag{31}$$

$$|^2\Delta_y\rangle = -\frac{1}{2}(|D_1\rangle + \sqrt{3}|D_2\rangle). \tag{32}$$

Therefore, the $|^2\Sigma^-\rangle$ and $|^2\Delta_y\rangle$ states can be described by X-TDA, even though they formally involve the double excitation $|\sigma\bar\pi_x\pi_y\rangle$. This has been achieved[4,5] through the $\bar\sigma \to \pi_y$ transition from the $M_s = -1/2$ component $|\sigma\bar\sigma\bar\pi_x\rangle$ of the tensor reference $\{|\sigma\bar\sigma\pi_x\rangle, |\sigma\bar\sigma\bar\pi_x\rangle\}$. The corresponding excitation energies indeed agree well with the MRCI and SF-TDA results. In contrast, U-TDA can only access the above $|D_1\rangle$ state and a spin-contaminated state $|TC\rangle$, which arises from the triplet-coupled single excitation of $|\sigma\bar\sigma\pi_x\rangle$ and is a 1:2 mixture of $|D_2\rangle$ and a quartet state $|Q\rangle$, i.e.,

$$|TC\rangle = \frac{1}{\sqrt{2}}(|\bar\sigma\pi_x\pi_y\rangle + |\sigma\pi_x\bar\pi_y\rangle) = \frac{1}{\sqrt{3}}(-|D_2\rangle + \sqrt{2}|Q\rangle), \tag{33}$$

TABLE IV. Spin multiplet states of open-shell molecules of CF, CH, and NH^+ by ROKS/TDA(A) and MRCI. The full SF-TDA results are in parentheses.

Molecule	Reference	Method	State	SVWN5	BLYP	B3LYP	CAM-B3LYP	BHHLYP	HF	MRCI
CF	$\|\sigma\pi_x\pi_y\rangle$	SF-TDA(A)	$^4\Sigma^-$	3.41	3.40 (3.55)	3.45 (3.59)	3.73 (3.86)	3.75 (3.91)	2.62	3.55
			$^2\Delta$	5.68	5.68 (5.74)	5.84 (5.89)	6.02 (6.06)	6.17 (6.22)	6.27	6.18
			$^2\Sigma^+$	6.85	6.70 (6.86)	6.88 (7.01)	6.96 (7.09)	7.09 (7.25)	7.92	7.25
			$^2\Sigma^-$	6.52	6.48 (6.58)	6.92 (7.02)	7.14 (7.24)	7.60 (7.72)	8.93	7.92
	$\|\sigma\bar{\sigma}\pi_x\rangle$	SF-TDA(A)	$^4\Sigma^-$	3.67	4.13	3.92	3.80	3.64	2.41	3.55
		X-TDA	$^2\Delta$	6.57	6.53	6.52	6.51	6.45	6.00	6.18
			$^2\Sigma^+$	6.77	6.84	6.89	6.96	6.42	6.37	6.71[a]
				6.97[b]	7.14[b]	7.25[b]	7.40[b]	6.38[b]	6.75[b]	7.25
			$^2\Sigma^-$	7.79	7.86	8.02	8.08	8.25	8.57	7.92
		U-TDA	$^2\Delta$	4.39	4.36	4.34	4.34	4.26	3.73	4.57[c]
			$^2\Sigma^+$	6.76	6.83	6.88	6.95	6.41	6.37	6.71[a]
			$^2\Sigma^-$	7.44	7.49	7.61	7.65	7.77	8.04	7.47[d]
CH	$\|\sigma\pi_x\pi_y\rangle$	SF-TDA(A)	$^4\Sigma^-$	0.50	0.71 (0.81)	0.80 (0.88)	0.98 (1.07)	1.10 (1.20)	0.10	0.75
			$^2\Delta$	2.57	2.66 (2.70)	2.75 (2.78)	2.85 (2.87)	2.96 (2.98)	2.90	2.89
			$^2\Sigma^-$	2.78	2.91 (2.92)	3.09 (3.09)	3.18 (3.17)	3.39 (3.38)	3.69	3.27
			$^2\Sigma^+$	3.85	3.75 (3.84)	3.83 (3.92)	3.84 (3.93)	3.93 (4.03)	4.59	3.96
	$\|\sigma\bar{\sigma}\pi_x\rangle$	SF-TDA(A)	$^4\Sigma^-$	0.55	1.22	1.03	0.86	0.83	−0.10	0.75
		X-TDA	$^2\Delta$	2.90	3.05	3.01	2.92	2.93	2.66	2.89
			$^2\Sigma^-$	3.11	3.33	3.35	3.27	3.38	3.39	3.27
			$^2\Sigma^+$	3.25	3.48	3.43	3.34	3.38	3.37	3.42[a]
				3.59[b]	3.92[b]	3.85[b]	3.77[b]	3.83[b]	4.08[b]	3.96
		U-TDA	$^2\Delta$	1.24	1.36	1.33	1.24	1.25	0.90	1.49[c]
			$^2\Sigma^-$	2.99	3.23	3.22	3.13	3.22	3.27	3.17[d]
			$^2\Sigma^+$	3.24	3.47	3.42	3.33	3.37	3.35	3.42[a]
NH^+	$\|\sigma\pi_x\pi_y\rangle$	SF-TDA(A)	$^4\Sigma^-$	−0.13	0.10 (0.20)	0.17 (0.25)	0.25 (0.35)	0.39 (0.50)	−0.61	0.04
			$^2\Delta$	2.69	2.82 (2.82)	2.84 (2.84)	2.89 (2.87)	2.96 (2.94)	2.80	2.96
			$^2\Sigma^-$	2.70	2.83 (2.78)	2.93 (2.88)	2.96 (2.91)	3.22 (3.04)	3.14	3.01
			$^2\Sigma^+$	4.58	4.46 (4.56)	4.47 (4.56)	4.45 (4.55)	4.46 (4.58)	5.12	4.46
	$\|\sigma\bar{\sigma}\pi_x\rangle$	SF-TDA(A)	$^4\Sigma^-$	−0.22	0.64	0.38	0.20	0.10	−0.10	0.04
		X-TDA	$^2\Delta$	2.95	3.03	2.95	2.85	2.81	2.53	2.96
			$^2\Sigma^-$	2.74	3.10	3.06	2.97	3.00	2.92	3.01
			$^2\Sigma^+$	3.50	3.82	3.71	3.61	3.60	3.57	3.71[a]
				4.06[b]	4.61[b]	4.47[b]	4.37[b]	4.38[b]	4.61[b]	4.46
		U-TDA	$^2\Delta$	0.71	0.86	0.79	0.70	0.65	0.31	1.02[c]
			$^2\Sigma^-$	2.76	3.06	2.99	2.90	2.93	2.89	3.00[d]
			$^2\Sigma^+$	3.50	3.82	3.70	3.61	3.59	3.55	3.71[a]

[a]Equation (40).
[b]Equation (41).
[c]Equation (38).
[d]Equation (37).

with

$$|Q\rangle = \frac{1}{\sqrt{3}}(|\bar{\sigma}\pi_x\pi_y\rangle + |\sigma\pi_x\bar{\pi}_y\rangle + \underline{|\sigma\bar{\pi}_x\pi_y\rangle}) \quad (34)$$

being the $M_s = 1/2$ component of $^4\Sigma^-$. In terms of the following relations:

$$|D_1\rangle = -\frac{1}{2}(\sqrt{3}|^2\Sigma^-\rangle + |^2\Delta_y\rangle), \quad (35)$$

$$|D_2\rangle = \frac{1}{2}(|^2\Sigma^-\rangle - \sqrt{3}|^2\Delta_y\rangle), \quad (36)$$

the excitation energies of $|D_1\rangle$ and $|TC\rangle$ can be written as

$$\omega[|D_1\rangle] = \frac{3}{4}\omega[|^2\Sigma^-\rangle] + \frac{1}{4}\omega[|^2\Delta_y\rangle], \quad (37)$$

$$\omega[|TC\rangle] = \frac{2}{3}\omega[|^4\Sigma^-\rangle] + \frac{1}{12}\omega[|^2\Sigma^-\rangle] + \frac{1}{4}\omega[|^2\Delta_y\rangle]. \quad (38)$$

It is seen from Table IV that the U-TDA energies for $^2\Delta$ and $^2\Sigma^-$, actually corresponding, respectively, to $|D_1\rangle$ and $|TC\rangle$, are indeed very close to the weighted MRCI values according to the right hand sides of Eqs. (37) and (38).

As X-TDA has only achieved spin but not space adaptation of TD-DFT, it still cannot correctly describe the $|^2\Sigma^+\rangle$ and $|^2\Delta_x\rangle$ states. Indeed, the X-TDA and U-TDA energies for $|^2\Sigma^+\rangle$ are virtually identical, and are both much lower than the MRCI results due to breaking of the space symmetry. A general remedy for this failure is to space-adapt TD-DFT for spatial degeneracy. This would mean that, in addition to $|\sigma\bar{\sigma}\pi_x\rangle$, the $|\sigma\bar{\sigma}\pi_y\rangle$ configuration, i.e., the y component of the $^2\Pi$ ground state, should also be included in the tensor reference. The required double excitation $|\sigma\bar{\pi}_y\pi_y\rangle$ then arises naturally from the $\bar{\sigma} \rightarrow \bar{\pi}_y$ single transition from $|\sigma\bar{\sigma}\pi_y\rangle$. Before such a space-adapted TD-DFT is formulated, a quick estimate of $|^2\Sigma^+\rangle$ can be made based on symmetry arguments. Using the following relations:

$$|\sigma\pi_x\bar{\pi}_x\rangle = \frac{1}{\sqrt{2}}(|^2\Sigma^+\rangle + |^2\Delta_x\rangle), \tag{39}$$

$$\omega[|\sigma\pi_x\bar{\pi}_x\rangle] = \frac{1}{2}\omega[|^2\Sigma^+\rangle] + \frac{1}{2}\omega[|^2\Delta_x\rangle], \tag{40}$$

the excitation energy for $|^2\Sigma^+\rangle$ can be estimated according to

$$\begin{aligned}\omega[|^2\Sigma^+\rangle] &= 2\omega[|\sigma\pi_x\bar{\pi}_x\rangle] - \omega[|^2\Delta_x\rangle] \\ &= 2\omega[|\sigma\pi_x\bar{\pi}_x\rangle] - \omega[|^2\Delta_y\rangle].\end{aligned} \tag{41}$$

Note that the degeneracy of the x and y components of the $^2\Delta$ state has been assumed here to arrive at the second equality. It is seen from Table IV that the so-corrected X-TDA energies for $|^2\Sigma^+\rangle$ indeed become in line with the MRCI values. Therefore, it can be expected that the rigorously space-adapted TD-DFT can provide more accurate results, just as X-TDA can improve U-TDA for spin-contaminated states.

Finally, it deserves to be mentioned that the EOM-CCSD (equation-of-motion coupled-cluster theory with singles and doubles) method fails completely for these excited states, for they all have significant double excitation characters. For instance, the UHF-EOM-CCSD energies[50] for the $^2\Sigma^-$ and $^2\Sigma^+$ states of CH are, respectively, 4.42 and 5.33 eV, far off compared with the present MRCI values of 3.27 and 3.96 eV. The corresponding results by CCSD-psT-LRT (spin-restricted open-shell coupled-cluster theory with singles, doubles, and pseudotriples linear response theory; 3.48 and 5.16 eV)[50] and CC3 (coupled cluster with iterative triples; 3.64 and 4.52 eV)[51] are also not very impressive. Only the CR-EOMCCSD(T) (completely renormalized EOM-CC with singles, doubles, and noniterative triples),[52] EA-EOMCCSDt (electron-attached EOMCCSDt),[53] EOM-CC(2,3) (EOM-CC model with single and double excitations in the CC part and single, double, and triple excitation in the EOM part),[54] and the spin-flip variants of EOM-CCSD and EOM-CC(2,3) (Ref. 54) can provide quantitative results. For example, the UHF-EOM-CC(2,3) energies[54] for the $^2\Sigma^-$ and $^2\Sigma^+$ states of CH are 3.33 and 4.11 eV, respectively, closely matching the corresponding MRCI values. However, these methods are computationally very expensive. In view of the high performance-cost ratio, SF-TD-DFT and X-TD-DFT should be regarded as promising tools for resolving spin multiplets of large open-shell systems.

V. CONCLUDING REMARKS

To gain deep insights on the formalism and performance of SF-TD-DFT, both the full and approximate noncollinear XC kernels have been closely examined in calculations of spatially degenerate or nearly degenerate systems as well as spin multiplets of closed- and open-shell systems. The results clearly demonstrate the necessity of using the full noncollinear hybrid kernel. However, the GGA part of the kernel might result in unsurmountable numerical instabilities in describing CV types of spin-flip transitions from an open-shell reference. Whenever this happens, the OO type of excitations are also affected indirectly. This defect can be remedied by the simple ALDA0 approximation, which is more accurate than the collinear XC kernels and computationally more efficient than the full noncollinear XC kernels. Moreover, SF-TD-DFT is also rather sensitive to the overlaps between the involved occupied and virtual orbitals, similar to the problem encountered in SC-TD-DFT for Rydberg or charge-transfer excitations. The situation can only be improved by mixing in a large amount of exact exchange in the functionals. Overall, due to its stability, accuracy, and efficiency, SF-TDA with the ALDA0 approximation to hybrid kernels can be recommended as a useful tool for excited state reactions and multiplet splittings.

There are still several limitations in the SF-TD-DFT formalism. First, only a limited number of configurations can be accessed. For instance, starting with a high-spin triplet reference, SF-TD-DFT can successfully handle all the four configurations (three singlets and one triplet) by distributing two electrons in two open-shell orbitals, something like CASCI(2,2) plus DFT dynamical correlation. However, if there exists an additional nearly degenerate orbital, the target singlet ground state cannot be obtained. A second common problem of SF-TD-DFT is the spin contamination in excited states. Most of the states investigated here arise predominantly from the OO($\alpha\beta$) or CV($\beta\alpha$) type of single excitations, which are automatically spin adapted. However, other types of spin-flip excitations, including CO($\alpha\beta$), OV($\alpha\beta$), and CV($\alpha\beta$), can be severely spin-contaminated. For such excitations, the spin-adapted SF-TD-DFT must be invoked. Progress along this line is being made in our laboratory.

ACKNOWLEDGMENTS

The research of this work was supported by grants from the National Natural Science Foundation of China (Project No. 21033001).

APPENDIX A: EVALUATION OF THE SPIN-FLIP GGA COUPLING MATRIX

1. Direct evaluation

The GGA XC potential $v^\sigma_{\rm XC}$ (15) can be written as

$$v^\sigma_{\rm XC} = v^\sigma_1 - 2v^\sigma_2 - 2v^\sigma_3 - v^\sigma_4 - v^\sigma_5, \tag{A1}$$

$$v^\sigma_1 = \frac{\partial e_{\rm XC}}{\partial \rho_\sigma}, \tag{A2}$$

$$\begin{aligned}v^\sigma_2 = {} & \frac{\partial^2 e_{\rm XC}}{\partial\rho_\sigma\partial\gamma_{\sigma\sigma}}\nabla\rho_\sigma\cdot\nabla\rho_\sigma + \frac{\partial^2 e_{\rm XC}}{\partial\rho_{\bar\sigma}\partial\gamma_{\sigma\sigma}}\nabla\rho_{\bar\sigma}\cdot\nabla\rho_\sigma \\ & + \frac{\partial^2 e_{XC}}{\partial\gamma_{\sigma\sigma}\partial\gamma_{\sigma\sigma}}\nabla\gamma_{\sigma\sigma}\cdot\nabla\rho_\sigma + \frac{\partial^2 e_{\rm XC}}{\partial\gamma_{\sigma\bar\sigma}\partial\gamma_{\sigma\sigma}}\nabla\gamma_{\sigma\bar\sigma}\cdot\nabla\rho_\sigma \\ & + \frac{\partial^2 e_{\rm XC}}{\partial\gamma_{\bar\sigma\bar\sigma}\partial\gamma_{\sigma\sigma}}\nabla\gamma_{\bar\sigma\bar\sigma}\cdot\nabla\rho_\sigma,\end{aligned} \tag{A3}$$

$$v^\sigma_3 = \frac{\partial e_{\rm XC}}{\partial\gamma_{\sigma\sigma}}\nabla^2\rho_\sigma, \tag{A4}$$

$$v_4^\sigma = \frac{\partial^2 e_{\rm XC}}{\partial\rho_\sigma\partial\gamma_{\sigma\bar\sigma}}\nabla\rho_\sigma\cdot\nabla\rho_{\bar\sigma} + \frac{\partial^2 e_{\rm XC}}{\partial\rho_{\bar\sigma}\partial\gamma_{\sigma\bar\sigma}}\nabla\rho_{\bar\sigma}\cdot\nabla\rho_{\bar\sigma} + \frac{\partial^2 e_{\rm XC}}{\partial\gamma_{\sigma\sigma}\partial\gamma_{\sigma\bar\sigma}}\nabla\gamma_{\sigma\sigma}\cdot\nabla\rho_{\bar\sigma} + \frac{\partial^2 e_{\rm XC}}{\partial\gamma_{\sigma\bar\sigma}\partial\gamma_{\sigma\bar\sigma}}\nabla\gamma_{\sigma\bar\sigma}\cdot\nabla\rho_{\bar\sigma} + \frac{\partial^2 e_{\rm XC}}{\partial\gamma_{\bar\sigma\bar\sigma}\partial\gamma_{\sigma\bar\sigma}}\nabla\gamma_{\bar\sigma\bar\sigma}\cdot\nabla\rho_{\bar\sigma}, \tag{A5}$$

$$v_5^\sigma = \frac{\partial e_{\rm XC}}{\partial\gamma_{\sigma\bar\sigma}}\nabla^2\rho_{\bar\sigma}. \tag{A6}$$

In terms of the pointwise potential $v_{\rm XC}^\sigma(\mathbf{r})$, Eq. (9) can be directly evaluated as it stands.

2. Integration by part

Invoking the integration by part, Eq. (9) can be evaluated equivalently as

$$[K_{\rm XC}^{\sigma\bar\sigma,\sigma\bar\sigma}]_{pq,rs} = \int \Omega_{pq}^{\sigma\bar\sigma}[(f_1-f_2)\Omega_{sr}^{\bar\sigma\sigma} + \vec{f}_3\cdot\nabla\Omega_{sr}^{\bar\sigma\sigma}]dV + \int \nabla\Omega_{pq}^{\sigma\bar\sigma}\cdot[\vec{f}_3\Omega_{sr}^{\bar\sigma\sigma}]dV, \tag{A7}$$

where

$$\Omega_{pq}^{\sigma\bar\sigma} = \psi_{p\sigma}\psi_{q\bar\sigma}, \tag{A8}$$

$$f_1 = \left(\frac{\partial e_{\rm XC}}{\partial\rho_\sigma} - \frac{\partial e_{\rm XC}}{\partial\rho_{\bar\sigma}}\right)(\rho_\sigma-\rho_{\bar\sigma})^{-1}, \tag{A9}$$

$$f_2 = \left(\frac{\partial e_{\rm XC}}{\partial\nabla\rho_\sigma} - \frac{\partial e_{\rm XC}}{\partial\nabla\rho_{\bar\sigma}}\right)\cdot(\nabla\rho_\sigma-\nabla\rho_{\bar\sigma})(\rho_\sigma-\rho_{\bar\sigma})^{-2} = \left[\left(2\frac{\partial e_{\rm XC}}{\partial\gamma_{\sigma\sigma}} - \frac{\partial e_{\rm XC}}{\partial\gamma_{\sigma\bar\sigma}}\right)(\gamma_{\sigma\sigma}-\gamma_{\sigma\bar\sigma}) + \left(2\frac{\partial e_{\rm XC}}{\partial\gamma_{\bar\sigma\bar\sigma}} - \frac{\partial e_{\rm XC}}{\partial\gamma_{\sigma\bar\sigma}}\right)(\gamma_{\bar\sigma\bar\sigma}-\gamma_{\sigma\bar\sigma})\right](\rho_\sigma-\rho_{\bar\sigma})^{-2}, \tag{A10}$$

$$\vec{f}_3 = \left(\frac{\partial e_{\rm XC}}{\partial\nabla\rho_\sigma} - \frac{\partial e_{\rm XC}}{\partial\nabla\rho_{\bar\sigma}}\right)(\rho_\sigma-\rho_{\bar\sigma})^{-1} = \left[\left(2\frac{\partial e_{\rm XC}}{\partial\gamma_{\sigma\sigma}} - \frac{\partial e_{\rm XC}}{\partial\gamma_{\sigma\bar\sigma}}\right)\nabla\rho_\sigma - \left(2\frac{\partial e_{\rm XC}}{\partial\gamma_{\bar\sigma\bar\sigma}} - \frac{\partial e_{\rm XC}}{\partial\gamma_{\sigma\bar\sigma}}\right)\nabla\rho_{\bar\sigma}\right]\times(\rho_\sigma-\rho_{\bar\sigma})^{-1}. \tag{A11}$$

APPENDIX B: ZERO EXCITATION ENERGY BY SF-RPA AND SF-TD-DFT

Herewith we prove a theorem, stating that both UKS-based SF-TD-DFT with the full noncollinear kernel and UHF-based SF-RPA shall yield a state exactly of zero excitation energy. The same holds only conditionally for ROKS-based SF-TD-DFT or ROHF-based SF-RPA.

1. The UHF/UKS case

The following convention for labeling the spatial parts of the spin orbitals is used for this section: $\{i, j, k, l, \dots\}$ for occupied, $\{a, b, c, d, \dots\}$ for unoccupied, and $\{p, q, r, s, \dots\}$ for unspecified α orbitals. The corresponding barred indices are for β orbitals. The spin step-down operator $\hat{S}_-$ takes the following form:

$$\hat{S}_- = \sum_p p_\beta^\dagger p_\alpha = \sum_{pq}\bar{q}_\beta^\dagger p_\alpha\lambda_{\bar q}^p, \quad \lambda_{\bar q}^p = \langle\bar q|p\rangle, \tag{B1}$$

where $p_\sigma^\dagger$ and p_σ are short-hand notations for creation and annihilation operators and $\lambda_{\bar q}^p$ are the overlaps between the spatial orbitals of different spins. The action of $\hat{S}_-$ on the high-spin UHF reference $|\Phi_0\rangle$ leads to

$$|\tilde\Phi_0\rangle \equiv \hat{S}_-|\Phi_0\rangle = \sum_{bj}|\Phi_j^{\bar b}\rangle\lambda_{\bar b}^j. \tag{B2}$$

The matrix element $\langle\Phi_i^{\bar a}|\hat H|\tilde\Phi_0\rangle$ can be evaluated as

$$\langle\Phi_i^{\bar a}|\hat H|\tilde\Phi_0\rangle = \langle\Phi_i^{\bar a}|\hat H\hat S_-|\Phi_0\rangle \tag{B3}$$

$$= \langle\Phi_i^{\bar a}|\hat S_-\hat H|\Phi_0\rangle \tag{B4}$$

$$= \langle\Phi_0|[i^\dagger\bar a, \hat S_-]\hat H|\Phi_0\rangle + \langle\Phi_0|\hat S_- i^\dagger\bar a\hat H|\Phi_0\rangle \tag{B5}$$

$$= \langle\Phi_0|\hat H|\Phi_0\rangle\lambda_{\bar a}^i + \langle\Phi_i^b|\hat H|\Phi_0\rangle\lambda_{\bar a}^b - \langle\Phi_{\bar j}^{\bar a}|\hat H|\Phi_0\rangle\lambda_{\bar j}^i + \sum_{bj}\langle\Phi_{i\bar j}^{\bar a b}|\hat H|\Phi_0\rangle\lambda_{\bar j}^b \tag{B6}$$

$$= \langle\Phi_0|\hat H|\Phi_0\rangle\lambda_{\bar a}^i + \sum_{bj}\langle\Phi_{i\bar j}^{\bar a b}|\hat H|\Phi_0\rangle\lambda_{\bar j}^b, \tag{B7}$$

where the last equality arises from the Brillouin conditions

$$F_{bi}^\alpha = \langle\Phi_i^b|\hat H|\Phi_0\rangle = 0, \quad F_{\bar a\bar j}^\beta = \langle\Phi_{\bar j}^{\bar a}|\hat H|\Phi_0\rangle = 0. \tag{B8}$$

Further applying the second equality of (B2) to the left hand side of Eq. (B7) leads to

$$\sum_{bj}\langle\Phi_i^{\bar a}|\hat H|\Phi_j^{\bar b}\rangle\lambda_{\bar b}^j - \langle\Phi_0|\hat H|\Phi_0\rangle\lambda_{\bar a}^i - \sum_{bj}\langle\Phi_{i\bar j}^{\bar a b}|\hat H|\Phi_0\rangle\lambda_{\bar j}^b = 0, \tag{B9}$$

which can be rewritten as

$$\sum_{bj}\langle\Phi_0|[(\bar a^\dagger i)^\dagger, [\hat H, \bar b^\dagger j]]|\Phi_0\rangle\lambda_{\bar b}^j - \sum_{bj}\langle\Phi_0|[(\bar a^\dagger i)^\dagger, \bar j^\dagger b]]|\Phi_0\rangle\lambda_{\bar j}^b = 0. \tag{B10}$$

The first and second expectation values are just the $\mathbf{A}^{\beta\alpha,\beta\alpha}$ and $\mathbf{B}^{\beta\alpha,\alpha\beta}$ matrices of SF-RPA. To draw analogy with Eqs. (11) and (12), we define

$$[\mathbf{X}_I^{\beta\alpha}]_{ai} = \lambda_{\bar a}^i = \langle\bar a|i\rangle, \quad [\mathbf{Y}_I^{\alpha\beta}]_{ai} = -\lambda_{\bar i}^a = -\langle\bar i|a\rangle. \tag{B11}$$

Equation (B10) then becomes

$$\mathbf{A}^{\beta\alpha,\beta\alpha}\mathbf{X}_I^{\beta\alpha} + \mathbf{B}^{\beta\alpha,\alpha\beta}\mathbf{Y}_I^{\beta\alpha} = 0. \tag{B12}$$

On the other hand, we would obtain the following relation:

$$\mathbf{B}^{\alpha\beta,\beta\alpha*}\mathbf{X}_I^{\beta\alpha} + \mathbf{A}^{\alpha\beta,\alpha\beta*}\mathbf{Y}_I^{\beta\alpha} = 0 \tag{B13}$$

by stating with the matrix element $\langle \hat{S}_+\Phi_0|\hat{H}|\Phi_{\bar{i}}^a\rangle$. Therefore, we have proved that the vector defined in Eq. (B11) satisfies Eq. (1) with zero eigenvalue. The proof is valid for both complex and real orbitals.

To see if the above finding also holds for UKS-based SF-TD-DFT, we consider one of the two expressions obtained by inserting Eq. (B11) into the left hand side of Eq. (1),

$$[\mathbf{A}^{\beta\alpha,\beta\alpha}\mathbf{X}_I^{\beta\alpha} + \mathbf{B}^{\beta\alpha,\alpha\beta}\mathbf{Y}_I^{\beta\alpha}]_{\bar{b}j} = \sum_{bj}[(\delta_{ij}F_{\bar{a}\bar{b}}^{\beta} - \delta_{ab}F_{ji}^{\alpha} + K_{\bar{a}i,\bar{b}j})\lambda_{\bar{b}}^{j} - K_{\bar{a}i,\bar{j}b}\lambda_{\bar{j}}^{b}], \tag{B14}$$

$$= \sum_b F_{\bar{a}\bar{b}}^{\beta}\langle\bar{b}|i\rangle - \sum_j \langle\bar{a}|j\rangle F_{ji}^{\alpha} + \sum_{bj}(K_{\bar{a}i,\bar{b}j}\lambda_{\bar{b}}^{j} - K_{\bar{a}i,\bar{j}b}\lambda_{\bar{j}}^{b}) \tag{B15}$$

$$= \langle\bar{a}|\hat{F}^{\beta} - \hat{F}^{\alpha}|i\rangle + \sum_{bj}(K_{\bar{a}i,\bar{b}j}\lambda_{\bar{b}}^{j} - K_{\bar{a}i,\bar{j}b}\lambda_{\bar{j}}^{b}), \tag{B16}$$

where the last equality arises from both the Brillouin conditions $F_{\bar{a}\bar{i}}^{\beta} = F_{ai}^{\alpha} = 0$ and the completeness relations $\sum_p |p\rangle\langle p| = \sum_p |\bar{p}\rangle\langle\bar{p}| = 1$. Since both GH and RSH functionals are just linear combinations of pure density functionals and HF exchange, we need to consider only the pure density functional case. Thus, the first term in Eq. (B16) can be written as

$$\langle\bar{a}|\hat{F}^{\beta} - \hat{F}^{\alpha}|i\rangle = \int \psi_{\bar{a}}^*(v_{\mathrm{XC}}^{\beta} - v_{\mathrm{XC}}^{\alpha})\psi_i dV \tag{B17}$$

$$= \int \psi_{\bar{a}}^*\psi_i \frac{v_{\mathrm{XC}}^{\beta} - v_{\mathrm{XC}}^{\alpha}}{\rho^{\beta} - \rho^{\alpha}}(\rho^{\beta} - \rho^{\alpha})dV \tag{B18}$$

$$= \int \psi_{\bar{a}}^*\psi_i f_{\mathrm{XC}}^{\beta\alpha}(\rho^{\beta} - \rho^{\alpha})dV. \tag{B19}$$

Note that

$$\rho^{\beta} - \rho^{\alpha} = \sum_j |\psi_{\bar{j}}|^2 - \sum_j |\psi_j|^2 \tag{B20}$$

$$= \sum_{pj}(\psi_p^*\psi_{\bar{j}}\lambda_{\bar{j}}^{p} - \psi_j^*\psi_{\bar{p}}\lambda_{\bar{p}}^{j}) \tag{B21}$$

$$= \sum_{bj}\left(\psi_b^*\psi_{\bar{j}}\lambda_{\bar{j}}^{b} - \psi_j^*\psi_{\bar{b}}\lambda_{\bar{b}}^{j}\right), \tag{B22}$$

where the last equality is due to cancelation of the occupied α and β orbitals. Thus, Eq. (B19) becomes

$$\langle\bar{a}|\hat{F}^{\beta} - \hat{F}^{\alpha}|i\rangle = \sum_{bj}\int \psi_{\bar{a}}^*\psi_i f_{\mathrm{XC}}^{\beta\alpha}\left(\psi_b^*\psi_{\bar{j}}\lambda_{\bar{j}}^{b} - \psi_j^*\psi_{\bar{b}}\lambda_{\bar{b}}^{j}\right)dV \tag{B23}$$

$$= \sum_{bj}(K_{\bar{a}i,\bar{j}b}\lambda_{\bar{j}}^{b} - K_{\bar{a}i,\bar{b}j}\lambda_{\bar{b}}^{j}), \tag{B24}$$

which is just the negative of the second term of Eq. (B16). That is, Eq. (B12) also holds for UKS-based SF-TD-DFT with the full noncollinear kernel. Equation (B13) can be proven in the same way. Therefore, both UKS-based SF-TD-DFT and UHF-based SF-RPA must have a zero eigenvalue with the corresponding eigenvector equation (B11).

2. The ROHF/ROKS case

The following convention is used here for the ROHF/ROKS spatial orbitals: $\{i, j, k, l, \dots\}$ for doubly occupied, $\{t, u, v, w, \dots\}$ for singly occupied, $\{a, b, c, d, \dots\}$ for unoccupied, and $\{p, q, r, s, \dots\}$ for unspecified orbitals. The symbol like $\bar{p}$ is used for spin orbitals of β electrons. Greek indices are used for spins.

Due to different Brillouin conditions, Eq. (B7) does not hold for the high-spin ROHF/ROKS reference $|\Phi_0\rangle = |S_i S_i\rangle$. However, we can still consider the matrix element

$$\langle\hat{S}_-\Phi_0|\hat{H}|\Phi_p^{\bar{q}}\rangle = \langle\Phi_0|\hat{S}_+\hat{H}|\Phi_p^{\bar{q}}\rangle \tag{B25}$$

$$= \langle\Phi_0|\hat{H}\hat{S}_+|\Phi_p^{\bar{q}}\rangle \tag{B26}$$

$$= \langle\Phi_0|\hat{H}\hat{S}_+T_{qp}^{\dagger}(1,-1)|\Phi_0\rangle \tag{B27}$$

$$= \langle\Phi_0|\hat{H}[\hat{S}_+, T_{qp}^{\dagger}(1,-1)]|\Phi_0\rangle + \langle\Phi_0|\hat{H}T_{qp}^{\dagger}(1,-1)\hat{S}_+|\Phi_0\rangle \tag{B28}$$

$$= \sqrt{2}\langle\Phi_0|\hat{H}T_{qp}^{\dagger}(1,0)|\Phi_0\rangle, \tag{B29}$$

where the identity $\hat{S}_+|\Phi_0\rangle = 0$ and the triplet-coupled spin-tensor operators[4]

$$T_{pq}^{\dagger}(1,-1) = p_{\beta}^{\dagger}q_{\alpha}, \tag{B30}$$

$$T_{pq}^{\dagger}(1,0) = \frac{1}{\sqrt{2}}(p_{\alpha}^{\dagger}q_{\alpha} - p_{\beta}^{\dagger}q_{\beta}) \tag{B31}$$

have been used. In view of the relation

$$\hat{S}_-|\Phi_0\rangle = \sum_t |\Phi_t^{\bar{i}}\rangle = \sqrt{2S_i}|S_i, S_i - 1\rangle, \tag{B32}$$

Eq. (B29) leads to

$$\mathrm{OO}(\alpha\beta): \langle\hat{S}_-\Phi_0|\hat{H}|\Phi_t^{\bar{u}}\rangle = \sqrt{2}\langle\Phi_0|\hat{H}T_{ut}^{\dagger}(1,0)|\Phi_0\rangle = \delta_{ut}\langle\Phi_0|\hat{H}|\Phi_u^{u}\rangle = \delta_{ut}\langle\Phi_0|\hat{H}|\Phi_0\rangle, \tag{B33}$$

$$\mathrm{CO}(\alpha\beta): \langle\hat{S}_-\Phi_0|\hat{H}|\Phi_i^{\bar{u}}\rangle = \sqrt{2}\langle\Phi_0|\hat{H}T_{ui}^{\dagger}(1,0)|\Phi_0\rangle = \langle\Phi_0|\hat{H}|\Phi_{\bar{i}}^{\bar{u}}\rangle = F_{iu}^{\beta} = 0, \tag{B34}$$

$$\mathrm{OV}(\alpha\beta): \langle\hat{S}_-\Phi_0|\hat{H}|\Phi_u^{\bar{a}}\rangle = \sqrt{2}\langle\Phi_0|\hat{H}T_{au}^{\dagger}(1,0)|\Phi_0\rangle = \langle\Phi_0|\hat{H}|\Phi_u^{a}\rangle = F_{ua}^{\alpha} = 0, \tag{B35}$$

$$\begin{aligned} \mathrm{CV}(\alpha\beta) : \langle \hat{S}_- \Phi_0 | \hat{H} | \Phi_i^{\bar{a}} \rangle &= \sqrt{2} \langle \Phi_0 | \hat{H} T_{ai}^{\dagger}(1,0) | \Phi_0 \rangle \\ &= \langle \Phi_0 | \hat{H} | \Phi_i^a \rangle - \langle \Phi_0 | \hat{H} | \Phi_{\bar{i}}^{\bar{a}} \rangle \\ &= 2F_{ia}^{\alpha}, \end{aligned} \tag{B36}$$

where use of the Brillouin conditions

$$F_{iu}^{\beta} = 0, \quad F_{ua}^{\alpha} = 0, \quad F_{ia}^{\alpha} + F_{ia}^{\beta} = 0, \tag{B37}$$

has been made. It is well known that the configuration space spanned by the $\mathrm{OO}(\alpha\beta)$ type of excitations is invariant under the action of $\hat{S}^2$. The invariance will be broken if the configurations generated by the $\mathrm{CO}(\alpha\beta)$ and $\mathrm{OV}(\alpha\beta)$ types of excitations are included, since they are mixed spin states. However, such configurations do not interact with $\hat{S}_-|\Phi_0\rangle$ due to the Brillouin conditions, see Eqs. (B34) and (B35). Thus, even if they are included, $\hat{S}_-|\Phi_0\rangle$ will still be a solution of the SF-CIS equation with zero excitation energy. The same conclusion can also be proved for SF-TDA with the full noncollinear kernel. However, once the configurations from the $\mathrm{CV}(\alpha\beta)$ type of excitations are included, $\hat{S}_-|\Phi_0\rangle$ will be mixed with $|\Phi_i^{\bar{a}}\rangle$ (see Eq. (B36)), thereby leading to a negative excitation energy for the lower component $|S_i, S_i - 1\rangle$. This is indeed what has been found numerically, see Table II. The pure spin symmetry and hence the degeneracy between $|\Phi_0\rangle$ and $\hat{S}_-|\Phi_0\rangle$ can only be resumed if additional doubles ($|\Phi_{it}^{a\bar{t}}\rangle$ and $|\Phi_{\bar{i}\bar{t}}^{\bar{a}\bar{t}}\rangle$) and triples $|\Phi_{itu}^{a\bar{t}\bar{u}}\rangle$ are further included. This is precisely what has been achieved by the spin-adapted RPA and TD-DFT (Ref. 4) for excited states of spin $S_i - 1$.

[1] Y. Shao, M. Head-Gordon, and A. I. Krylov, J. Chem. Phys. **118**, 4807 (2003).
[2] N. Minezawa and M. S. Gordon, J. Phys. Chem. A **113**, 12749 (2009); **115**, 901 (2011).
[3] B. G. Levine, C. Ko, J. Quenneville, and T. J. Martínez, Mol. Phys. **104**, 1039 (2006).
[4] Z. Li and W. Liu, J. Chem. Phys. **133**, 064106 (2010).
[5] Z. Li, W. Liu, Y. Zhang, and B. Suo, J. Chem. Phys. **134**, 134101 (2011).
[6] F. Wang and T. Ziegler, J. Chem. Phys. **121**, 12191 (2004).
[7] F. Wang and T. Ziegler, J. Chem. Phys. **122**, 074109 (2005).
[8] F. Wang and W. Liu, J. Chin. Chem. Soc. (Taipei) **50**, 597 (2003).
[9] J. Gao, W. Liu, B. Song, and C. Liu, J. Chem. Phys. **121**, 6658 (2004).
[10] J. Gao, W. Zou, W. Liu, Y. Xiao, D. Peng, B. Song, and C. Liu, J. Chem. Phys. **123**, 054102 (2005).
[11] D. Peng, W. Zou, and W. Liu, J. Chem. Phys. **123**, 144101 (2005).
[12] M. Seth, G. Mazur, and T. Ziegler, Theor. Chem. Acc. **129**, 331 (2011).
[13] M. Huix-Rotllant, B. Natarajan, A. Ipatov, C. M. Wawire, T. Deutsch, and M. E. Casida, Phys. Chem. Chem. Phys. **12**, 12811 (2010).
[14] Z. Rinkevicius and H. Ågren, Chem. Phys. Lett. **491**, 132 (2010).
[15] Z. Rinkevicius, O. Vahtras, and H. Ågren, J. Chem. Phys. **133**, 114104 (2010).
[16] O. Vahtras and Z. Rinkevicius, J. Chem. Phys. **126**, 114101 (2007).
[17] J. S. Sears, C. D. Sherrill, and A. I. Krylov, J. Chem. Phys. **118**, 9084 (2003).
[18] Z. Li and W. Liu, J. Chem. Phys. **135**, 194106 (2011).
[19] R. E. Stratmann, G. E. Scuseria, and M. J. Frisch, J. Chem. Phys. **109**, 8218 (1998).
[20] S. Hirata and M. Head-Gordon, Chem. Phys. Lett. **314**, 291 (1999).
[21] N. J. Russ, T. D. Crawford, and G. S. Tschumper, J. Chem. Phys. **120**, 7298 (2004).
[22] R. Bast, H. J. Aa Jensen, and T. Saue, Int. J. Quantum Chem. **109**, 2091 (2009).
[23] T. Yanai, D. P. Tew, and N. C. Handy, Chem. Phys. Lett. **393**, 51 (2004).
[24] C. Lee, W. Yang, and R. G. Parr, Phys. Rev. B **37**, 785 (1988).
[25] W. Liu, G. Hong, D. Dai, L. Li, and M. Dolg, Theor. Chem. Acc. **96**, 75 (1997).
[26] W. Liu, F. Wang, and L. Li, J. Theor. Comput. Chem. **2**, 257 (2003).
[27] W. Liu, F. Wang, and L. Li, in Recent Advances in Relativistic Molecular Theory, Recent Advances in Computational Chemistry Vol. 5, edited by K. Hirao and Y. Ishikawa, (World Scientific, Singapore, 2004), p. 257.
[28] W. Liu, F. Wang, and L. Li, in *Encyclopedia of Computational Chemistry*, electronic edition, edited by P. von Ragué Schleyer, N. L. Allinger, T. Clark, J. Gasteiger, P. A. Kollman, H. F. Schaefer III, and P. R. Schreiner (Wiley, Chichester, UK, 2004).
[29] S. H. Vosko, L. Wilk, and M. Nusair, Can. J. Phys. **58**, 1200 (1980).
[30] A. D. Becke, Phys. Rev. A **38**, 3098 (1988).
[31] A. D. Becke, J. Chem. Phys. **98**, 5648 (1993).
[32] P. J. Stephens, F. J. Devlin, C. F. Chabalowski, and M. J. Frisch, J. Phys. Chem. **98**, 11623 (1994).
[33] A. I. Krylov, Chem. Phys. Lett. **338**, 375 (2001).
[34] Y. Wang, G. Zhai, B. Suo, Z. Gan, and Z. Wen, Chem. Phys. Lett. **375**, 134 (2003).
[35] Y. Wang, H. Han, G. Zhai, B. Suo, and Z. Wen, Sci. China, Ser. B: Chem. **47**, 276 (2004).
[36] B. Suo, G. Zhai, Y. Wang, Z. Wen, X. Hu, and L. Li, J. Comput. Chem. **26**, 88 (2005).
[37] S. Huzinaga, J. Chem. Phys. **42**, 1293 (1965); T. H. Dunning, *ibid.* **53**, 2823 (1970); **55**, 716 (1971).
[38] A. I. Krylov and C. D. Sherrill, J. Chem. Phys. **116**, 3194 (2002).
[39] F. Cordova, L. J. Doriol, A. Ipatov, M. E. Casida, C. Filippi, and A. Vela, J. Chem. Phys. **127**, 164111 (2007).
[40] R. Krishnan, J. S. Binkley, R. Seeger, and J. A. Pople, J. Chem. Phys. **72**, 650 (1980).
[41] T. H. Dunning, Jr., J. Chem. Phys. **90**, 1007 (1989).
[42] R. J. Buenker and S. D. Peyerimhoff, Chem. Phys. Lett. **29**, 253 (1974).
[43] C. M. Hadad, J. B. Foresman, and K. B. Wiberg, J. Phys. Chem. **97**, 4293 (1993).
[44] K. B. Wiberg, C. M. Hadad, J. B. Foresman, and W. A. Chupka, J. Phys. Chem. **96**, 10756 (1992).
[45] M. J. G. Peach, P. Benfield, T. Helgaker, and D. J. Tozer, J. Chem. Phys. **128**, 044118 (2008).
[46] C. Hu, O. Sugnio, and Y. Miyamoto, Phys. Rev. A **74**, 032508 (2006).
[47] C. Hu and O. Sugnio, J. Chem. Phys. **126**, 074112 (2007).
[48] K. Yang, R. Peverati, D. G. Truhlar, and R. Valero, J. Chem. Phys. **135**, 044118 (2011).
[49] K. P. Huber and G. Herzberg, *Molecular Spectra and Molecular Structure*, Constants of Diatomic Molecules Vol. IV (Van Nostrand, New York, 1979).
[50] P. G. Szalay and J. Gauss, J. Chem. Phys. **112**, 4027 (2000).
[51] C. E. Smith, R. A. King, and T. D. Crawford, J. Chem. Phys. **122**, 054110 (2005).
[52] M. Włoch, J. R. Gour, K. Kowalski, and P. Pieuch, J. Chem. Phys. **122**, 214107 (2005).
[53] J. R. Gour, P. Piecuch, and M. Włoch, J. Chem. Phys. **123**, 134113 (2005).
[54] L. V. Slipchenko and A. I. Krylov, J. Chem. Phys. **123**, 084107 (2005).